Analytic-normal-mode frequencies for N identical particles: The microscopic dynamics underlying the emergence and stability of excitation gaps from BCS to unitarity

D. K. Watson *

Homer L. Dodge Department of Physics and Astronomy, University of Oklahoma, Norman, Oklahoma 73019, USA

(Received 21 May 2021; accepted 18 August 2021; published 27 September 2021)

The frequencies of the analytic normal modes for N identical particles are studied as a function of system parameters from the weakly interacting BCS regime to the strongly interacting unitary regime. The normal modes were obtained previously from a first-order $L = 0$ group theoretic solution of a three-dimensional Hamiltonian with a general two-body interaction for confined identical particles. In a precursor to this study, the collective behavior of these normal modes was investigated as a function of N from few-body systems to many-body systems analyzing the contribution of individual particles to the collective macroscopic motions. A specific case, the Hamiltonian for Fermi gases in the unitary regime, was studied in more detail. This regime is known to support collective behavior in the form of superfluidity and has previously been successfully described using normal modes. Two phenomena that could sustain the emergence and stability of superfluid behavior were revealed, including the behavior of the normal mode frequencies as N increases. In this paper, I focus on a more detailed analysis of these analytic frequencies, extending my investigation to include Hamiltonians with a range of interparticle interaction strengths from the BCS regime to the unitary regime and analyzing the microscopic dynamics that lead to large gaps at unitarity. The results of the present study suggest that in regimes where higher-order effects are small, normal modes can be used to describe the physics of superfluidity from the weakly interacting BCS regime with the emergence of small excitation gaps to unitarity with its large gaps and can offer insight into a possible microscopic understanding of the behavior at unitarity. This approach could thus offer an alternative to the two-body pairing models commonly used to describe superfluidity along this transition.

DOI: 10.1103/PhysRevA.104.033320

I. INTRODUCTION

The evolution of collective behavior in the form of superfluidity for systems of ultracold gaseous fermions from the BCS regime to unitarity has been studied intensely during the past two decades since this transition was first explored in the laboratory [1–9]. Typically, theoretical methods assume that fermions are pairing into loosely bound Cooper pairs in the BCS regime to explain the emergence of superfluid behavior [10–16]. As the interparticle interaction increases toward the unitary regime in ultracold fermion gases, these atomic Cooper pairs decrease in size, ultimately forming diatomic molecules that condense in the Bose-Einstein condensation (BEC) regime on the other side of unitarity. In materials supporting superconductivity, the emergence of Cooper pairs of electrons is mediated by interactions with phonons in the underlying material creating a weak attraction that can bind two electrons at long distances [10–14]. In an ultracold Fermi gas, neutral atoms are assumed to pair at large distances due to weak interactions when a Feshbach resonance is tuned far from resonance. In this study, I will present an alternative possibility to describe the transition from the weakly interacting BCS regime to the strong interactions of the unitary regime that does not assume that individual fermions are forming pairs. Instead, the proposed model assumes many-body pairing exhibited through normal modes to model the physics, i.e., synchronized collisionless motion of the particles that makes it impossible to know which fermion is paired with any other fermion. Normal mode functions naturally provide simple, coherent macroscopic wave functions with phase coherence that is maintained over the entire ensemble. The excitations between modes define quasiparticles of the macroscopic quantum system. I will show how the two lowest normal mode frequencies relevant for ultracold systems, a gapless phonon mode with extremely low frequencies and a particle-hole excitation mode, exhibit, as expected, an extremely small excitation gap in the weakly interacting BCS regime, which widens as the interaction increases, reaching a maximum in the unitary regime. The physics of this model from BCS to unitarity is a precursor to the physical pairing of atoms in real space that eventually forms diatomic molecules in the BEC region.

Normal mode behavior is ubiquitous in the universe, occurring at all scales from the vibration of crystals [17] to the oscillation of rotating stars [18]. This universal dynamic reflects the widespread appearance of vibrational motions in nature [17–29], which can often be coupled into the simple collective motions of normal modes. These collective motions depend on the interparticle correlations of the system and thus incorporate many-body effects into simple dynamic motion. If higher-order effects are small, these collective motions are eigenfunctions of an approximate Hamiltonian and acquire some degree of stability as a function of time; thus a system in a single normal mode will tend to stay in that mode unless perturbed. Normal modes manifest the symmetry of

*dwatson@ou.edu

this underlying approximate Hamiltonian with the possibility of offering analytic solutions to many-body problems and a clear physical picture of the microscopic dynamics underlying diverse phenomena.

In an earlier paper, I studied the character of five types of normal modes previously derived as the $L = 0$ first-order analytic solutions of a general Hamiltonian for confined identical particles [30] using a perturbation formalism called symmetry-invariant perturbation theory (SPT) [31–38]. Using the simple analytic expressions for the N-body normal-mode coordinates, I investigated the evolution of their physical character as a function of N, from few-body to many-body systems, and examined the motion of the individual particles as they contributed to the collective motion. Some general observations were made based on symmetry considerations and then their behavior was analyzed for a specific case, the Hamiltonian of a confined system of fermions in the unitary regime, which is known to support superfluid behavior. This study found that the behavior expected for few-body systems, which have the well-known motions of molecular equivalents such as ammonia and methane (symmetric stretch, symmetric bend, antisymmetric stretch, antisymmetric bend, and the opening and closing of alternative interparticle angles), evolves smoothly as N increases to the collective motions expected for large-N ensembles (breathing, center of mass, particle-hole radial and angular excitations, and phonon). Furthermore, the transition from few-body behavior to large-N behavior was found to occur at quite low values of N ($N \approx 10$). This change in character from small N to large N is dictated by fairly simple analytic forms that nonetheless incorporate the intricate interplay of individual particles as they contribute to the macroscopic motion. The evolution of behavior was found to be determined primarily from the symmetry structure of the Hamiltonian and thus could be applicable to diverse phenomena at different scales if the same symmetry is present or dominates.

The SPT formalism was developed initially for systems of bosons [31–37] and more recently applied to fermions [38–41]. This approach has been formulated for $L = 0$ three-dimensional systems with spherically-symmetric confining potentials and completely general interaction potentials through first order in the perturbation series. Wave functions through first order have been developed and tested for systems of bosons [32,34–37], but not for fermions. The extension to higher orders has been formulated using an algorithm that uses tensor algebra [42]. The normal mode solutions, which are the exact solutions at first order, are used as a complete basis to obtain expansion coefficients for the energy and wave function at each order. This extension, while straightforward, is quite challenging particularly in memory requirements, reflecting the exponential growth in complexity as a function of perturbation order (not the value of N) that has been demonstrated for this method [43,44], and has not been implemented for large-N systems which have many degrees of freedom [42]. Higher-order calculations for the energies of small atomic systems have been carried out in earlier versions of this approach [45–49], as well as the extension and application to higher angular momentum states [50–54]. The extension to cylindrically confined systems has been formulated, but not implemented.

The SPT formalism at each order takes into account every two-body interaction rather than some average interaction and is applicable to strongly interacting systems since the perturbation parameter does not involve the interaction potential. Beyond-mean-field effects are included even at the lowest perturbation order underpinning the excellent results obtained through first order using the SPT approach [33,38,41] as well as earlier dimensional methods [45,46,55–57].

This formalism has also been tested against an exactly solvable model problem of harmonically interacting particles under harmonic confinement [36,37,39,40]. Exact agreement was found (to ten or more digits of accuracy) for the wave function with the exact analytic wave function obtained in an independent solution, confirming this general formalism for a fully interacting three-dimensional N-body system [36] and verifying the analytic expressions for the normal mode frequencies and coordinates.

In the fermion studies, the numerically demanding determination of explicitly antisymmetrized wave functions is avoided by using specific assignments of normal mode occupations to enforce the Pauli principle at first order "on paper" [38–41] [see Sec. II after Eq. (18)]. Ground- [38] and excited-state [41] beyond-mean-field energies and their degeneracies have been determined, allowing the construction of a partition function [40,41] and the determination of thermodynamic quantities [40,41]. Constructing the partition function required a large number of excited states from the infinite spectrum of equally spaced states, chosen specifically to comply with the enforcement of the Pauli principle, thus connecting the Pauli principle to many-body interaction dynamics through the normal modes.

The study of the thermodynamic behavior of ultracold fermions in the unitary regime obtained quite good agreement with experimental data for the energy, entropy, and heat capacity [41]. Two normal modes, selected by the Pauli principle, were found to play a role in creating and stabilizing the superfluid behavior at low temperatures, a phonon mode at ultralow temperatures, and a single-particle excitation mode, i.e., a particle-hole excitation, as the temperature increases. The single-particle excitation has a much higher frequency and creates a gap that stabilizes the superfluid behavior. This normal mode description offers an interesting alternative to two-body pairing correlation models commonly used to describe superfluid regimes.

The good agreement with experiment for thermodynamic quantities increased the interest in investigating the physical character of these states. Originally obtained simply as a complete basis at first order, these states offer the possibility of acquiring physical intuition into the dynamics of collective motion [30] and insight into the universal behavior of the unitary regime.

My previous study of the five types of normal mode coordinates looked at the evolution of behavior as a function of N for only one specific case, the strongly interacting unitary regime. This region was chosen because of the current experimental and theoretical interest in this regime, which is known to exhibit universal behavior and to support superfluidity with large excitation gaps. My analysis of the N dependence for the unitary Hamiltonian revealed two phenomena that have the potential to support the creation and stabilization of collective

behavior. First the mixing of radial and angular behavior in the normal modes is found to limit to pure radial or pure angular behavior for very large (or very small) N. This results in symmetry coordinates that are eigenfunctions of an approximate Hamiltonian governing the physics of the unitary regime, thus acquiring some amount of stability if the symmetry is unperturbed. Second, for low values of N, the five types of normal mode frequencies start out closer in value, but as N increases these frequencies spread out, creating large gaps between the values of these five frequencies. These gaps could provide the stability for superfluid behavior if mechanisms to prevent the transfer of energy to other modes exist (such as low temperatures) or could be engineered.

In this paper, I extend my investigation to regimes other than the unitary regime, studying the evolution of the frequencies as a function of the interparticle interaction strength $\bar{V}_0$ from the BCS regime to unitarity. I will focus on larger values of N relevant to experimental investigations of this transition. For this study, I have scaled the value of $\bar{V}_0$ so that $\bar{V}_0 = 1.0$ corresponds to the unitary regime which has an infinite scattering length. The BCS regime is loosely defined as having extremely weak interparticle interactions, e.g., $\bar{V}_0 \approx 10^{-6}$. This potential is defined in Sec. II, with a more detailed description in Appendix A in Ref. [30].

The analytic expressions for the five types of frequencies have a complicated dependence on $\bar{V}_0$, both explicitly and implicitly through other variables in the formalism that depend on $\bar{V}_0$. The goal is to determine the interplay of various terms in the Hamiltonian as they respond to the increase in the interparticle interaction and affect the value of the frequencies. This understanding should offer insight into the microscopic dynamics that leads to large gaps as unitarity is approached and offers the possibility of fine-tuning the system parameters to control the appearance and stability of excitation gaps.

In the remainder of this section, I summarize the results of my investigation and state my conclusions. Section II gives a brief review of the SPT method including the derivation of the symmetry coordinates, the normal coordinates, and the normal mode frequencies, establishing the necessary notation. Section III looks at the mixing coefficients (defined in Appendix A) that determine the radial-angular mixing of the symmetry coordinates to form a normal coordinate, extending my earlier study in the unitary regime to regimes with weak interactions. Similar behavior is found for all strengths of the interparticle interaction. Specifically, the character of the normal modes $q_{\pm}^{\prime[\alpha]}$ evolves to almost purely radial or purely angular as N increases, with very little mixing of the symmetry coordinates, confirming that this phenomenon is driven by dynamics other than the universal behavior of a system at unitarity. This negligible mixing is reflected in the character of the normal mode frequencies, which can be appropriately labeled as radial frequencies or angular frequencies across the entire transition. It also has implications for the ability to tune these frequencies as well as the stability of collective behavior since the symmetry coordinates are eigenfunctions of an approximate underlying Hamiltonian.

In Sec. IV and Appendixes B–E, I analyze the analytic expressions for the five types of frequencies in terms of their dependence on $\bar{V}_0$, confirming that the frequencies can be characterized into two types: radial frequencies that have a strong dependence on $\bar{V}_0$ and angular frequencies with a weaker dependence on $\bar{V}_0$ that evolve to stable limits insensitive to changes in $\bar{V}_0$.

Section V discusses the behavior of the frequencies and the emergence of stable gaps as a function of $\bar{V}_0$ from the BCS regime to the unitary regime. This analysis shows the emergence of excitation gaps that increase as $\bar{V}_0$ increases. For extremely weak interactions, the five frequencies converge to identical values at twice the trap frequency, which results in infinitesimally small excitation gaps. As $\bar{V}_0$ increases, the frequencies begin to spread out, creating gaps that reach a maximum at unitarity with the angular frequencies approaching stable limits while the radial frequencies continue to gradually change. (These limits are derived in detail in Appendixes F and G). For ultracold systems, the two lowest frequencies are of interest: the phonon frequency, which tends to extremely small values, and the angular particle-hole frequency, which limits to the trap frequency at unitarity. This sets up an excitation gap that stabilizes as the unitary limit is approached. As N increases, this behavior is stabilized at smaller and smaller values of $\bar{V}_0$. Since $\bar{V}_0$ appears as a parameter in the analytic expressions for the frequencies, the evolution of these frequencies can be studied as a function of the interparticle interaction without intensive numerical work.

Finally, in Sec. VI, the microscopic dynamics underpinning the stable limits of the angular frequencies and the emergence of excitation gaps that could support superfluidity are investigated from two perspectives. First the relative contributions of various Hamiltonian terms to the evolving analytic frequencies are tracked as $\bar{V}_0$ changes. Then the motion of the individual particles in the corresponding normal mode coordinate is studied to understand how the ensemble is rearranging on a microscopic level as interactions turn on and collective behavior emerges. The excitation gap relevant for ultracold Fermi gases limits to the trap frequency at unitarity, setting up a spectrum of evenly spaced levels identical to the spectrum of the noninteracting regime. This results in dynamics independent of microscopic details of the underlying interactions consistent with the universal behavior of the unitary regime.

In summary, this study of the evolution of the normal mode frequencies from the first-order solution of the SPT equations for confined systems of identical particles as a function of $\bar{V}_0$ suggests that these normal modes are able to describe the physics of superfluidity from the weakly interacting BCS regime to the universal behavior of unitarity and to offer a view of the microscopic dynamics without the assumption of two-particle pairing.

II. SYMMETRY-INVARIANT PERTURBATION THEORY: DERIVATION OF NORMAL MODES AND THEIR FREQUENCIES

In this section, I summarize the development of SPT and the previous derivation of the normal modes and their frequencies that was presented in Refs. [31,32], introducing the notation required in Secs. III–VI for the analysis of the frequencies.

The normal modes are the exact solutions at first order in inverse dimensionality of a first-principles perturbation

many-body formalism called symmetry-invariant perturbation theory. This formalism uses group theory to solve a fully interacting many-body three-dimensional Hamiltonian with a confining potential and an arbitrary interaction potential [32,35]. Using the symmetry of the symmetric group at large dimension [31], this group theoretic approach successfully rearranges the many-body work at each perturbation order so that an exact solution can in principle be obtained non-numerically, order by order, using group theory and graphical techniques [43]. Specifically, the numerical work is rearranged into analytic building blocks, resulting in a formulation with a complexity that does not scale with N [35–37,43,44]. Group theory is used to partition the N scaling problem away from the interaction dynamics, allowing the N scaling to be treated as a separate mathematical problem (cf. the Wigner-Eckart theorem). The exponential scaling in complexity is shifted from a dependence on the number of particles N to a dependence on the order of the perturbation series [44]. Exact first-order results that contain beyond-mean-field effects for all values of N can now be obtained from a single calculation, but determining higher-order results becomes exponentially difficult. To minimize the work needed for new calculations, the analytic building blocks have been calculated and stored [58].

Strongly interacting systems like the unitary regime can be studied since the perturbation does not involve the strength of the interaction. Beyond unitarity, as a system of ultracold Fermi gases transitions into the BEC regime, the normal mode first-order basis with its many-body pairing is not a useful basis to describe the transition to diatomic molecules with two-body pairing. This BEC regime could in principle be described by including higher-order terms in the series, although it is probable that many terms would be required, making convergence challenging and undermining the ability to obtain physical insight.

The Schrödinger equation in D dimensions is defined in Cartesian coordinates for N interacting particles by

$$H\Psi = \left[\sum_{i=1}^{N} h_i + \sum_{i=1}^{N-1}\sum_{j=i+1}^{N} g_{ij}\right]\Psi = E\Psi, \tag{1}$$

$$h_i = -\frac{\hbar^2}{2m_i}\sum_{\nu=1}^{D}\frac{\partial^2}{\partial x_{i\nu}^2} + V_{\rm conf}\left(\sqrt{\sum_{\nu=1}^{D} x_{i\nu}^2}\right),$$

$$g_{ij} = V_{\rm int}\left(\sqrt{\sum_{\nu=1}^{D}(x_{i\nu}-x_{j\nu})^2}\right), \tag{2}$$

where h_i is the single-particle Hamiltonian, g_{ij} is a two-body interaction potential, $x_{i\nu}$ is the νth Cartesian component of the ith particle, and $V_{\rm conf}$ is a spherically-symmetric confining potential [31,32,35]. The Schrödinger equation is transformed from Cartesian coordinates to internal coordinates using

$$r_i = \sqrt{\sum_{\nu=1}^{D} x_{i\nu}^2} \quad (1 \leqslant i \leqslant N),$$

$$\gamma_{ij} = \cos(\theta_{ij}) = \left(\sum_{\nu=1}^{D} x_{i\nu}x_{j\nu}\right)\Big/ r_i r_j \tag{3}$$

$(1 \leqslant i < j \leqslant N)$, which are the D-dimensional scalar radii r_i of the N particles from the center of the confining potential and the cosines γ_{ij} of the $N(N-1)/2$ angles between the radial vectors.

The first-order derivatives are removed using a similarity transformation [59], and dimensionally-scaled oscillator length units are defined with a length scale factor $\kappa(D) = D^2\bar{a}_{\rm ho}$, where $\bar{a}_{\rm ho} = \sqrt{\frac{\hbar}{m\bar{\omega}_{\rm ho}}}$ and $\bar{\omega}_{\rm ho} = D^3\omega_{\rm ho}$, that regularizes the large-dimension limit of the Schrödinger equation. Substituting the scaled variables $\bar{r}_i = r_i/\kappa(D)$, with $\bar{E} = D^2\frac{E}{\hbar\bar{\omega}_{\rm ho}}$ and $\bar{H} = D^2\frac{H}{\hbar\bar{\omega}_{\rm ho}}$, into the similarity-transformed Schrödinger equation gives

$$\bar{H}\Phi = (\delta^2\bar{T} + \bar{U} + \bar{V}_{\rm conf} + \bar{V}_{\rm int})\Phi = \bar{E}\,\Phi, \tag{4}$$

where

$$\bar{T} = \sum_{i=1}^{N}\left(-\frac{1}{2}\frac{\partial^2}{\partial\bar{r}_i^{\,2}} - \frac{1}{2\bar{r}_i^2}\sum_{j\neq i}\sum_{k\neq i}\frac{\partial}{\partial\gamma_{ij}} \times (\gamma_{jk} - \gamma_{ij}\gamma_{ik})\frac{\partial}{\partial\gamma_{ik}}\right), \tag{5}$$

$$\bar{U} = \sum_{i=1}^{N}\left(\frac{\delta^2 N(N-2) + [1-\delta(N+1)]^2\left(\frac{\Gamma^{(i)}}{\Gamma}\right)}{8\bar{r}_i^2}\right), \tag{6}$$

$$\bar{V}_{\rm conf} = \sum_{i=1}^{N}\frac{1}{2}\bar{r}_i^2, \tag{7}$$

$$\bar{V}_{\rm int} = \frac{\bar{V}_0}{1-3b'\delta}\sum_{i=1}^{N-1}\sum_{j=i+1}^{N}(1-\tanh\Theta_{ij}), \tag{8}$$

$\hbar = m = 1$, $\delta = 1/D$ is the perturbation parameter, Γ is the Gramian determinant with elements γ_{ij} (see Appendix D in Ref. [31]), and $\Gamma^{(i)}$ is the determinant with the row and column of the ith particle deleted. The barred quantities have been scaled by $\kappa(D)$.

The form of the interaction potential $\bar{V}_{\rm int}$ is chosen to reduce to a square-well potential at $D = 3$ and to be differentiable away from $D = 3$ to allow the dimensional analysis [31,33]. The constant b' in the denominator is chosen so the potential yields an infinite scattering length for the unitary regime with $\bar{V}_0 = 1.0$. To evolve toward the weaker interactions of the BCS regime, $\bar{V}_0$ is scaled to smaller values. The argument Θ_{ij} is defined as

$$\Theta_{ij} = \frac{\bar{c}_0}{1-3\delta}\left(\frac{\bar{r}_{ij}}{\sqrt{2}} - \bar{\alpha} - 3\delta(\bar{R}-\bar{\alpha})\right), \tag{9}$$

where $\bar{r}_{ij}$ is the interatomic separation

$$\bar{r}_{ij} = \sqrt{\bar{r}_i^2 + \bar{r}_j^2 - 2\bar{r}_i\bar{r}_j\gamma_{ij}}, \tag{10}$$

$\bar{R}$ is the range of the square-well potential in dimensionally scaled oscillator units, and $\bar{\alpha}$ is a constant which softens the potential as $D \to \infty$. The range R is chosen so $R \ll a_{\rm ho}$ ($a_{\rm ho} = \sqrt{\hbar/m\omega_{\rm ho}}$) and has been systematically reduced to extrapolate to zero-range interaction.

Taking the $D \to \infty$ limit, the second derivative terms drop out, yielding a static zeroth-order problem with an effective

potential $\bar{V}_{\rm eff}$:

$$\bar{V}_{\rm eff}(\bar{r},\gamma;\delta)=\sum_{i=1}^{N}[\bar{U}(\bar{r}_i;\delta)+\bar{V}_{\rm conf}(\bar{r}_i;\delta)]+\sum_{i=1}^{N-1}\sum_{j=i+1}^{N}\bar{V}_{\rm int}(\bar{r}_i,\gamma_{ij};\delta). \tag{11}$$

The minimum of this effective potential yields an infinite-dimensional maximally-symmetric structure with all radii $\bar{r}_i$ and angle cosines γ_{ij} of the particles equal, i.e., when $D\to\infty$, $\bar{r}_i=\bar{r}_\infty$ $(1\leqslant i\leqslant N)$ and $\gamma_{ij}=\gamma_\infty$ $(1\leqslant i<j\leqslant N)$. The values of these parameters are determined by two minimum conditions

$$\left(\frac{\partial\bar{V}_{\rm eff}}{\partial\bar{r}_i}\right)\Big|_\infty=0,\quad \left(\frac{\partial\bar{V}_{\rm eff}}{\partial\gamma_{ij}}\right)\Big|_\infty=0. \tag{12}$$

Substituting the above definition of $\bar{V}_{\rm eff}$, two equations in $\bar{r}_\infty$ and γ_∞ are obtained which yield

$$\bar{r}_\infty=\frac{1}{\sqrt{2}\sqrt{1+(N-1)\gamma_\infty}}, \tag{13}$$

while γ_∞ can be solved from the transcendental equation

$$\frac{\gamma_\infty[2+(N-2)\gamma_\infty]}{(1-\gamma_\infty)^{3/2}\sqrt{1+(N-1)\gamma_\infty}}+\bar{V}_0\,\mathrm{sech}^2(\Theta_\infty)\Theta'_\infty=0. \tag{14}$$

In the large-D limit ($\delta\to0$), the argument Θ_{ij} becomes

$$\Theta_\infty=\Theta_{ij}|_\infty=\bar{c}_0(\sqrt{1-\gamma_\infty}\,\bar{r}_\infty-\bar{\alpha}). \tag{15}$$

The zeroth-order energy at this minimum, $\bar{E}_\infty=\bar{V}_{\rm eff}(\bar{r}_\infty)$, provides the starting point for the $1/D$ expansion. A position vector of the $N(N+1)/2$ internal coordinates is defined as

$$\bar{\boldsymbol{y}}=\begin{pmatrix}\bar{\boldsymbol{r}}\\ \gamma\end{pmatrix}, \tag{16}$$

where

$$\gamma=\begin{pmatrix}\gamma_{12}\\ \gamma_{13}\\ \gamma_{23}\\ \gamma_{14}\\ \gamma_{24}\\ \gamma_{34}\\ \gamma_{15}\\ \gamma_{25}\\ \vdots\\ \gamma_{N-2,N}\\ \gamma_{N-1,N}\end{pmatrix},\quad \bar{\boldsymbol{r}}=\begin{pmatrix}\bar{r}_1\\ \bar{r}_2\\ \vdots\\ \bar{r}_N\end{pmatrix}.$$

The substitutions $\bar{r}_i=\bar{r}_\infty+\delta^{1/2}\bar{r}'_i$ and $\gamma_{ij}=\gamma_\infty+\delta^{1/2}\gamma'_{ij}$ set up a power series in $\delta^{1/2}$ about the $D\to\infty$ symmetric minimum.

The first-order $\delta=1/D$ equation is a harmonic problem, which is solved exactly and analytically by obtaining the N-body normal modes of the system. The first-order Hamiltonian $\bar{H}_1$ is defined in terms of constant matrices $\boldsymbol{G}$ and $\boldsymbol{F}$ that are evaluated at the large-dimension limit

$$\bar{H}_1=-\tfrac{1}{2}\partial_{\bar{\boldsymbol{y}}'}{}^T\boldsymbol{G}\partial_{\bar{\boldsymbol{y}}'}+\tfrac{1}{2}\bar{\boldsymbol{y}}'^T\boldsymbol{F}\bar{\boldsymbol{y}}'+v_0, \tag{17}$$

where G involves kinetic energy terms, F involves derivatives of the effective potential, and v_0 is a constant [31]. The FG matrix method [60] is used to obtain the normal mode frequencies and the harmonic-order energy correction [31]. A review of the FG matrix method is presented in Appendix A of Ref. [31]. Here $N(N+1)/2$ frequencies $\bar{\omega}$ are obtained from the roots of the FG equation; however, only five roots are distinct due to the large degeneracy of the frequencies reflecting the very high degree of symmetry manifested in the $\boldsymbol{F}$, $\boldsymbol{G}$, and $\boldsymbol{FG}$ matrices. The elements of these matrices are evaluated for the large-dimension maximally-symmetric structure with a single value for all radii $\bar{r}_\infty$ and angle cosines γ_∞. Thus these matrices are invariant under the $N!$ operations of particle interchanges effected by the symmetric group S_N, which results in the highly degenerate eigenvalues. These matrices do not connect subspaces belonging to different irreducible representations of S_N [61] (see, for example, Ref. [60], Appendix XII, p. 347); thus the normal coordinates must transform under irreducible representations of S_N.

There are a total of five irreducible representations: two one-dimensional irreducible representations, one radial and one angular, labeled by the partition $[N]$; two $(N-1)$-dimensional irreducible representations, one radial and one angular, labeled by the partition $[N-1,1]$; and one angular $N(N-3)/2$-dimensional irreducible representation, labeled by the partition $[N-2,2]$. These representations are given shorthand labels $\mathbf{0}^-$, $\mathbf{0}^+$, $\mathbf{1}^-$, $\mathbf{1}^+$, and $\mathbf{2}$, respectively (see Refs. [32,35]). Thus the energy through first order in $\delta=1/D$ can be written in terms of the five distinct normal mode frequencies [31,55] as

$$\overline{E}=\overline{E}_\infty+\delta\left[\sum_{\mu=\{\mathbf{0}^\pm,\mathbf{1}^\pm,\mathbf{2}\}}\left(n_\mu+\frac{1}{2}d_\mu\right)\bar{\omega}_\mu+v_0\right], \tag{18}$$

where μ is a label which runs over the five types of normal modes $\mathbf{0}^-$, $\mathbf{0}^+$, $\mathbf{1}^-$, $\mathbf{1}^+$, and $\mathbf{2}$ [irrespective of the particle number (see Ref. [31] and Ref. [15] in [32])], n_μ is the total quanta in the normal mode with frequency $\bar{\omega}_\mu$, and v_0 is a constant [defined in Ref. [31], Eq. (125)]. The multiplicities of the five roots are $d_{\mathbf{0}^+}=1$, $d_{\mathbf{0}^-}=1$, $d_{\mathbf{1}^+}=N-1$, $d_{\mathbf{1}^-}=N-1$, and $d_{\mathbf{2}}=N(N-3)/2$.

The energy expression given by Eq. (18) gives the ground-state energy as well as the excited-state spectrum by assigning normal mode quantum numbers consistent with the Pauli principle. The allowed assignments are determined by finding a correspondence between the normal mode states $|n_{\mathbf{0}^+},n_{\mathbf{0}^-},n_{\mathbf{1}^+},n_{\mathbf{1}^-},n_{\mathbf{2}}\rangle$ and the noninteracting states of the confining potential, a spherically-symmetric three-dimensional harmonic oscillator [$V_{\rm conf}(r_i)=\frac{1}{2}m\omega_{\rm ho}^2r_i^2$], which have known restrictions due to antisymmetry. These two spectra are related in the double limit $D\to\infty$ and $\omega_{\rm ho}\to\infty$ where both representations are valid. The radial and angular characters separate cleanly at this double limit, resulting in two conditions [38,39]

$$2n_{\mathbf{0}^-}+2n_{\mathbf{1}^-}=\sum_{i=1}^{N}2\nu_i,\quad 2n_{\mathbf{0}^+}+2n_{\mathbf{1}^+}+2n_{\mathbf{2}}=\sum_{i=1}^{N}l_i, \tag{19}$$

where ν_i is the radial and l_i is the orbital angular momentum quantum number of the three-dimensional harmonic

oscillator, satisfying $n_i = 2\nu_i + l_i$, and n_i is the energy-level quanta of the ith particle defined by $E = \sum_{i=1}^{N}[n_i + \frac{3}{2}]\hbar\omega_{\rm ho} = \sum_{i=1}^{N}[(2\nu_i + l_i) + \frac{3}{2}]\hbar\omega_{\rm ho}$.

Equations (19) determine a set of possible normal mode states $|n_{\mathbf{0}^+}, n_{\mathbf{0}^-}, n_{\mathbf{1}^+}, n_{\mathbf{1}^-}, n_{\mathbf{2}}\rangle$ that are consistent with an antisymmetric wave function from the known set of harmonic-oscillator configurations that obey the Pauli principle. As particles are added at the noninteracting $\omega_{\rm ho} \to \infty$ limit, additional harmonic-oscillator quanta ν_i and l_i are of course needed to satisfy the Pauli principle. Equivalently, this corresponds to additional normal mode quanta needed to maintain antisymmetry as interactions turn on and the normal modes reflect the emerging many-body interactions. This strategy is similar to Landau's use of the noninteracting system to set up the correct Fermi statistics as interactions adiabatically evolve in Fermi liquid theory [62].

We define the symmetry coordinate vector S as

$$\boldsymbol{S} = \begin{pmatrix} \boldsymbol{S}^{[N]}_{\bar{\boldsymbol{r}}'} \\ \boldsymbol{S}^{[N]}_{\boldsymbol{\gamma}'} \\ \boldsymbol{S}^{[N-1,1]}_{\bar{\boldsymbol{r}}'} \\ \boldsymbol{S}^{[N-1,1]}_{\boldsymbol{\gamma}'} \\ \boldsymbol{S}^{[N-2,2]}_{\boldsymbol{\gamma}'} \end{pmatrix} = \begin{pmatrix} W^{[N]}_{\bar{\boldsymbol{r}}'}\bar{\boldsymbol{r}}' \\ W^{[N]}_{\boldsymbol{\gamma}'}\boldsymbol{\gamma}' \\ W^{[N-1,1]}_{\bar{\boldsymbol{r}}'}\bar{\boldsymbol{r}}' \\ W^{[N-1,1]}_{\boldsymbol{\gamma}'}\boldsymbol{\gamma}' \\ W^{[N-2,2]}_{\boldsymbol{\gamma}'}\boldsymbol{\gamma}' \end{pmatrix}, \tag{20}$$

where the $W^{[\alpha]}_{\bar{\boldsymbol{r}}'}$ and the $W^{[\alpha]}_{\boldsymbol{\gamma}'}$ are transformation matrices. This is shown in Ref. [32] using the theory of group characters to decompose $\bar{\boldsymbol{r}}'$ and $\boldsymbol{\gamma}'$ into basis functions that transform under these five irreducible representations of S_N. The $\boldsymbol{FG}$ method is applied using these symmetry coordinates to determine the eigenvalues $\lambda_\alpha = \bar{\omega}^2_\alpha$, frequencies $\bar{\omega}_\alpha$, and normal modes $\boldsymbol{q}'^{[\alpha]}$ of the system

$$\boldsymbol{q}'^{[N]}_{\pm} = c^{[N]}_{\pm}\big(\cos\theta^{[N]}_{\pm}\big[\boldsymbol{S}^{[N]}_{\bar{\boldsymbol{r}}'}\big] + \sin\theta^{[N]}_{\pm}\big[\boldsymbol{S}^{[N]}_{\boldsymbol{\gamma}'}\big]\big), \tag{21}$$

$$\boldsymbol{q}'^{[N-1,1]}_{\xi\pm} = c^{[N-1,1]}_{\pm}\big(\cos\theta^{[N-1,1]}_{\pm}\big[\boldsymbol{S}^{[N-1,1]}_{\bar{\boldsymbol{r}}'}\big]_\xi + \sin\theta^{[N-1,1]}_{\pm}\big[\boldsymbol{S}^{[N-1,1]}_{\boldsymbol{\gamma}'}\big]_\xi\big) \tag{22}$$

for the $\alpha = [N]$ and $[N-1,1]$ sectors and $1 \leqslant \xi \leqslant N-1$ and

$$\boldsymbol{q}'^{[N-2,2]} = c^{[N-2,2]}\boldsymbol{S}^{[N-2,2]}_{\boldsymbol{\gamma}'} \tag{23}$$

for the $[N-2,2]$ sector.

From Eqs. (21) and (22) above, the symmetry coordinates in the $[N]$ and $[N-1,1]$ sectors are mixed to form a normal coordinate. Thus, depending on the value of the mixing angles, the normal modes, which are the eigenfunctions at first order of the Schrödinger equation, will have mixed radial and angular behavior in the $[N]$ and $[N-1,1]$ sectors. The $[N-2,2]$ normal modes have entirely angular behavior since there are no $\bar{\boldsymbol{r}}'$ symmetry coordinates in this sector and so no mixing. The value of the mixing angles and thus the extent of radial-angular mixing in a normal coordinate depends of course on the Hamiltonian terms at this first perturbation order.

III. MIXING COEFFICIENTS AS A FUNCTION OF N AND $\bar{V}_0$

The mixing coefficients that determine the radial-angular mixing in the normal modes for the $[N]$ and $[N-1,1]$ sectors are defined in Appendix A and have a complicated dependence on N and $\bar{V}_0$ that originates in the Hamiltonian terms at first order. In particular, these coefficients have some explicit dependence from the symmetry present in the first-order Hamiltonian as well as dependence from the F and G elements for a particular Hamiltonian.

As shown in Appendix A, there are three layers of analytic expressions that can introduce N and/or $\bar{V}_0$ dependence. When these mixing coefficients were plotted for the unitary (large-$\bar{V}_0$) Hamiltonian as a function of N in a recent study, the character of the normal modes was found to evolve to a pure radial or pure angular symmetry coordinate for $N \geqslant 200$, i.e., no mixing for $N \gg 1$. (This was also true for very small N, e.g., $N \leqslant 10$, which are not being studied in this work).

A bit of inspection revealed that this behavior was being dictated to a large extent by the explicit N dependence in the expressions for $\cos\theta^{[\alpha]}_{\pm}$ and $\sin\theta^{[\alpha]}_{\pm}$ [Eqs. (A1)–(A8)]. The expressions depend on the symmetry of the first-order Hamiltonian, not the specific details of the potential. The position and shape of the crossover is influenced by the other sources of N and $\bar{V}_0$ dependence that originate in the specific Hamiltonian.

The emergence of pure symmetry coordinates for large N has implications for the stability of collective behavior since the symmetry coordinates are eigenfunctions of an approximate underlying Hamiltonian and thus have some degree of stability unless the system is perturbed. In addition, this means that the frequencies $\bar{\omega}_{[N]^\pm}$ and $\bar{\omega}_{[N-1,1]^\pm}$ associated with these normal modes should reflect pure radial or pure angular character for large N.

In the present study, I now extend this earlier study to regimes other than the unitary regime, investigating whether this emergence of pure symmetry character in the normal modes and their frequencies is unique to the unitary regime or is driven by dynamics common to regimes throughout the transition from BCS to unitarity.

In Figs. 1(a)–1(d), I show the behavior of the mixing coefficients as a function of N for a system of identical fermions in the weakly interacting BCS regime, plotting the square of the mixing coefficients $|\cos\theta^{[\alpha]}_{\pm}|^2$ and $|\sin\theta^{[\alpha]}_{\pm}|^2$ which gives the probability associated with each symmetry coordinate $[\boldsymbol{S}^{[\alpha]}_{\bar{\boldsymbol{r}}'}]$ or $[\boldsymbol{S}^{[\alpha]}_{\boldsymbol{\gamma}'}]$ in the expression for the normal modes $q'^{[\alpha]}_{\pm}$. The plots show that the character of the normal modes $q'^{[\alpha]}_{\pm}$ evolves to almost purely radial or purely angular, as N increases with very little mixing of the symmetry coordinates. This happens in this weakly interacting regime at even lower values of N than in the unitary regime, thus confirming that this phenomenum is driven by dynamics other than the universal behavior of a system at unitarity. This also validates the decision to designate the $[N]$ and $[N-1,1]$ sector normal mode frequencies for the typical many-body ensemble sizes studied in the laboratory, as either a radial frequency or an angular frequency instead of having mixed radial-angular character. Inspecting the plots reveals that $\bar{\omega}_{0^+}$ and $\bar{\omega}_{1^+}$ are

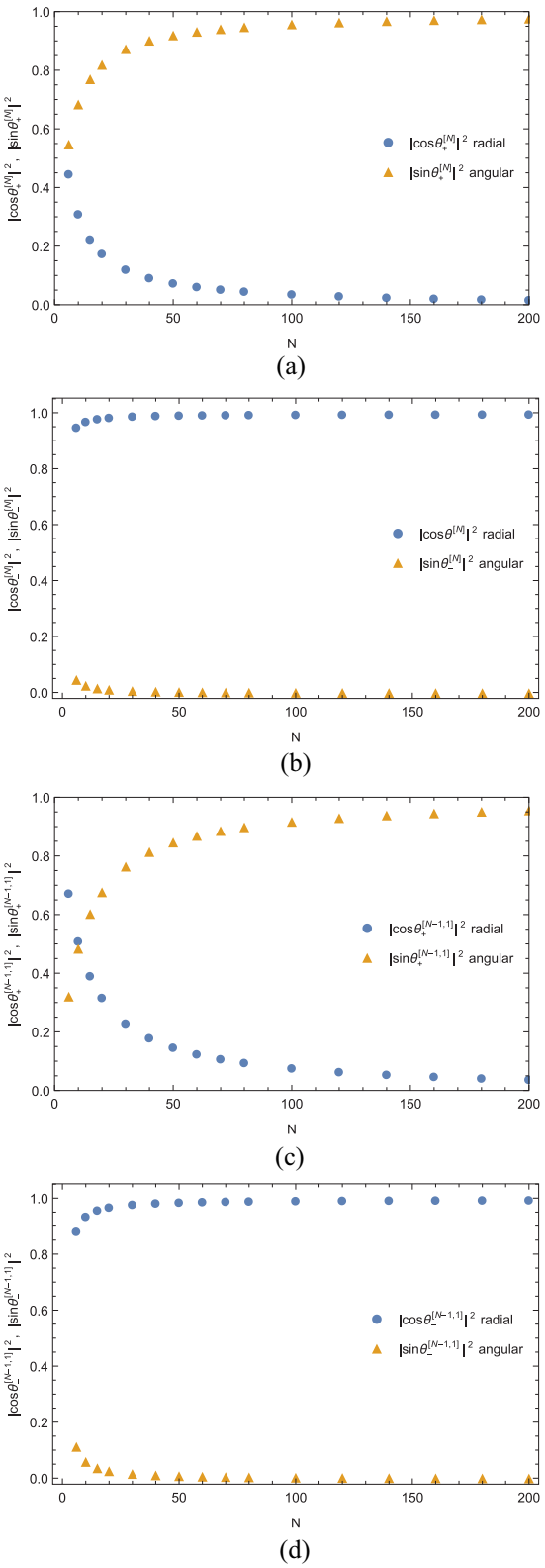

FIG. 1. Square of the mixing coefficients as a function of N for the weakly interacting BCS regime: (a) $|\cos\theta_+^{[N]}|^2$ and $|\sin\theta_+^{[N]}|^2$ for the normal mode $q_+'^{[N]}$, (b) $|\cos\theta_-^{[N]}|^2$ and $|\sin\theta_-^{[N]}|^2$ for the normal mode $q_-'^{[N]}$, (c) $|\cos\theta_+^{[N-1,1]}|^2$ and $|\sin\theta_+^{[N-1,1]}|^2$ for $q_+'^{[N-1,1]}$, and (d) $|\cos\theta_-^{[N-1,1]}|^2$ and $|\sin\theta_-^{[N-1,1]}|^2$ for $q_-'^{[N-1,1]}$.

angular frequencies and $\bar{\omega}_{0^-}$ and $\bar{\omega}_{1^-}$ are radial frequencies. (This designation holds over the entire range of interparticle interaction strengths until the systems are approaching the unitary regime where the large value of $\bar{V}_0$ results in a crossing of the character at which point the labels are switched).

IV. ANALYTIC EXPRESSIONS FOR THE FIVE NORMAL MODE FREQUENCIES

In this section, I analyze the analytic expressions for the frequencies, investigating the differences between the radial ($\bar{\omega}_{0^-}$ and $\bar{\omega}_{1^-}$) and angular ($\bar{\omega}_{0^+}$ and $\bar{\omega}_{1^+}$) frequencies in the $[N]$ and $[N-1,1]$ sectors, as well as studying the angular frequency $\bar{\omega}_2$ in the $[N-2,2]$ sector. The radial frequencies depend strongly on the interparticle interaction potential $\bar{V}_0$, while the angular frequencies which are comprised primarily from centrifugal potential terms have a weaker dependence on $\bar{V}_0$. Thus all the frequencies will respond to tuning the interaction strength in the laboratory using a Feshbach resonance.

Analytic expressions for the N-body normal mode frequencies were derived in Ref. [31] using a method outlined in Appendixes B and C of that paper, which derives analytic formulas for the roots λ_μ of the FG secular equation. The normal mode vibrational frequencies $\bar{\omega}_\mu^2$ are related to the roots λ_μ of $\boldsymbol{FG}$ by

$$\lambda_\mu = \bar{\omega}_\mu^2. \tag{24}$$

The two frequencies associated with the λ_0 roots of multiplicity 1 are of the form

$$\bar{\omega}_{0^\pm} = \sqrt{\eta_0 \mp \sqrt{{\eta_0}^2 - \Delta_0}}, \tag{25}$$

where

$$\eta_0 = \frac{1}{2}\left[a + (N-1)b + g + 2(N-2)h + \frac{(N-2)(N-3)}{2}\iota\right]$$
$$\Delta_0 = [a + (N-1)b]\left[g + 2(N-2)h + \frac{(N-2)(N-3)}{2}\iota\right]$$
$$- \frac{N-1}{2}[2c + (N-2)d][2e + (N-2)f]. \tag{26}$$

For the two $N-1$ multiplicity roots, the frequencies are

$$\bar{\omega}_{1^\pm} = \sqrt{\eta_1 \mp \sqrt{{\eta_1}^2 - \Delta_1}}, \tag{27}$$

where η_1 and Δ_1 are given by

$$\eta_1 = \tfrac{1}{2}[a - b + g + (N-4)h - (N-3)\iota],$$
$$\Delta_1 = -(N-2)(c-d)(e-f) + (a-b)$$
$$\times [g + (N-4)h - (N-3)\iota]. \tag{28}$$

The frequency $\bar{\omega}_2$, associated with the root λ_2 of multiplicity $N(N-3)/2$, is given by

$$\bar{\omega}_2 = \sqrt{g - 2h + \iota}. \tag{29}$$

The quantities a, b, c, d, e, f, g, h, and ι are defined in Appendix B in terms of the F and G elements of the first-order Hamiltonian.

Explicit $\bar{V}_0$ dependence in the analytic expressions for the frequencies. Analogous to the mixing coefficients, there are three layers of analytic expressions that define the frequencies: the expressions for $\bar{\omega}_{0^\pm}$, $\bar{\omega}_{1^\pm}$, and $\bar{\omega}_2$ in Eqs. (25)–(29) above, the expressions for a, b, c, d, e, f, g, h, and ι given in Appendix B, and the expressions for the F and G elements of Eq. (17) which are also given in Appendix B. The expressions for $\bar{\omega}_{0^\pm}$, $\bar{\omega}_{1^\pm}$, and $\bar{\omega}_2$ do not contain $\bar{V}_0$ explicitly, however the next layer, which involves the quantities a, b, c, d, e, f, g, h, and ι, does have an explicit dependence on $\bar{V}_0$, as well as the third layer involving the F and G elements of the first-order Hamiltonian.

Implicit dependence of the frequencies on $\bar{V}_0$ through the variables $\bar{r}_\infty$, γ_∞, $\tanh\Theta_\infty$, and $\mathrm{sech}^2\Theta_\infty$. The frequencies have some implicit dependence on $\bar{V}_0$ from the variables $\bar{r}_\infty$ and γ_∞ whose values are obtained as roots of transcendental equations that involve $\bar{V}_0$ [see Eqs. (12)–(14)]. The values of $\bar{r}_\infty$ and γ_∞ are also used to determine $\tanh\Theta_\infty$ and $\mathrm{sech}^2\Theta_\infty$. This implicit dependence on the interparticle interaction strength through the solution of transcendental equations complicates understanding the dependence of the frequencies on $\bar{V}_0$ solely by analytic means, however it is possible with a little numerical work to understand how $\bar{V}_0$ is implicitly affecting the frequencies through these variables.

A. The $[N]$ sector frequencies $\bar{\omega}_{0^\pm}$

The normal mode frequencies in the $[N]$ sector, $\bar{\omega}_{0^+}$ and $\bar{\omega}_{0^-}$, are associated with the angular center-of-mass mode and the radial breathing mode, respectively. These two frequencies are the largest frequencies of the five normal modes and so do not come into play in providing an excitation gap in ultracold regimes. It is interesting to analyze the relative contributions of the interaction potential $\bar{V}_0$ versus terms originating in the kinetic energy for these $[N]$ sector frequencies. The breathing frequency is expected to depend strongly on the strength of $\bar{V}_0$ as the particles spread out and then move back in toward the minimum of the effective potential. For the center-of-mass frequency, the dependence on $\bar{V}_0$ should drop out of the final simplified analytic expression since the center-of-mass mode is independent of interparticle interactions. In Appendix C, I demonstrate how the quadratic formula for $\bar{\omega}_{0^+}$ and $\bar{\omega}_{0^-}$ results in one frequency $\bar{\omega}_{0^-}$, the breathing mode, constructed from the terms at first order that involve $\bar{V}_0$ with the centrifugal terms from the kinetic energy canceling, while the other frequency $\bar{\omega}_{0^+}$, the center-of-mass mode, is constructed from centrifugal terms at first order with the terms that involve $\bar{V}_0$ canceling.

B. The $[N-1]$ sector frequencies $\bar{\omega}_{1^\pm}$

The normal mode frequencies in the $[N-1, 1]$ sector, $\bar{\omega}_{1^+}$ and $\bar{\omega}_{1^-}$, are associated with angular and radial particle-hole excitations. These two frequencies are the closest frequencies to the extremely low phonon frequency occupied in ultracold regimes and thus play a role in setting up an excitation gap for these systems. It is again enlightening to analyze the relative contributions of the interaction potential $\bar{V}_0$ versus the kinetic energy for these $[N-1, 1]$ sector frequencies. The radial particle-hole frequency should depend strongly on the strength of $\bar{V}_0$, as a single particle is excited from the ensemble in a radial direction. For the angular particle-hole excitation frequency, I expect to see the strong dependence on $\bar{V}_0$ drop out of the final simplified analytic expression and the centrifugal terms in the effective potential contribute. This is demonstrated in Appendix D.

C. The $[N-2, 2]$ sector frequency $\bar{\omega}_2$

The normal mode frequency in the $[N-2, 2]$ sector, $\bar{\omega}_2$, is associated with the phonon compressional mode which has an extremely small frequency and thus is the only normal mode occupied by a gas of fermions at ultracold temperatures. This is an angular mode, so I expect its frequency to be relatively independent of $\bar{V}_0$ and to have a strong dependence on centrifugal terms. This is shown in Appendix E.

V. EVOLUTION OF EXCITATION GAPS FROM WEAKLY INTERACTING TO UNITARITY

I discuss the emergence, growth, and stability of excitation gaps as the frequencies evolve as a function of the strength of interparticle interactions.

A. $\bar{V}_0$ increases for a fixed ensemble size

I fix the system size, i.e., the value of N, and let the interaction strength $\bar{V}_0$ increase. This analysis is directly relevant to experiments which use a Feshbach resonance to tune the interaction strength for a particular system. The value of $\bar{V}_0$ is changed from essentially zero, i.e., the case of independent noninteracting particles trapped in a harmonic potential, to the large interactions ($\bar{V}_0 = 1.0$) of the unitary regime.

Figures 2(a)–2(c) show this effect for $N = 10^3$, 10^4, and 10^5 particles, respectively, as $\bar{V}_0$ is tuned from the BCS regime to the unitary regime. The plots show that at the limit of zero interparticle interactions, the frequencies coalesce to the same value of $2\bar{\omega}_{\mathrm{ho}}$ as expected and observed in the laboratory [4,63]. [See an expanded view in Figs. 3(a)–3(c) of the region near the independent-particle limit]. As interactions are slowly turned on, gaps rapidly emerge, reaching values that stabilize for the angular frequencies as unitarity is approached.

Unlike the angular frequencies that quickly converge to limiting values, the radial frequencies continue to slowly increase as unitarity is approached, suggesting that higher-order terms are needed to converge the radial frequencies. The angular frequencies approach limits that are integer multiples of the trap frequency: twice the trap frequency for the center-of-mass angular frequency, $\bar{\omega}_{0^+} = 2\bar{\omega}_{\mathrm{ho}}$; equal to the trap frequency for the single-particle angular excitation, $\bar{\omega}_{1^+} = \bar{\omega}_{\mathrm{ho}}$; and orders of magnitude smaller than the trap frequency for the phonon mode, $\bar{\omega}_2 = O(10^{-2})\bar{\omega}_{\mathrm{ho}}$. For $N \gg 1$, stable values for the angular frequencies are reached quite quickly as $\bar{V}_0$ increases from the BCS regime. [See Figs. 3(a)–3(c)].

As can be seen in all the above figures, the largest gap forms between the extremely-low-frequency phonon mode, which is the only mode occupied by ultracold gases, and the

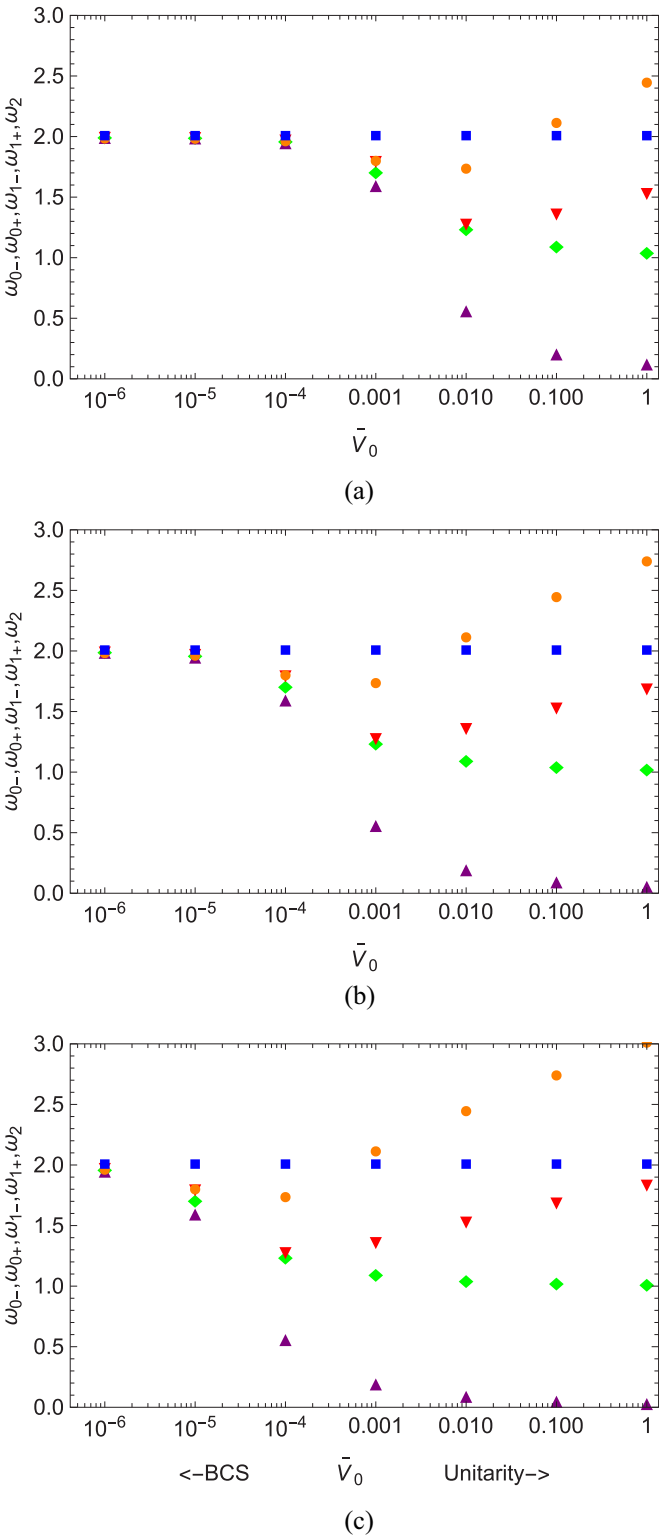

FIG. 2. Frequencies as a function of the interparticle interaction strength $\bar{V}_0$ from BCS to unitarity in units of the trap frequency (ω_{0^-}, orange circles; ω_{0^+}, blue squares; ω_{1^-}, red down triangles; ω_{1^+}, green diamonds; and ω_2, purple up triangles) for (a) $N = 10^3$ fermions, (b) $N = 10^4$ fermions, and (c) $N = 10^5$ fermions. Note the logarithmic scale on the x axis.

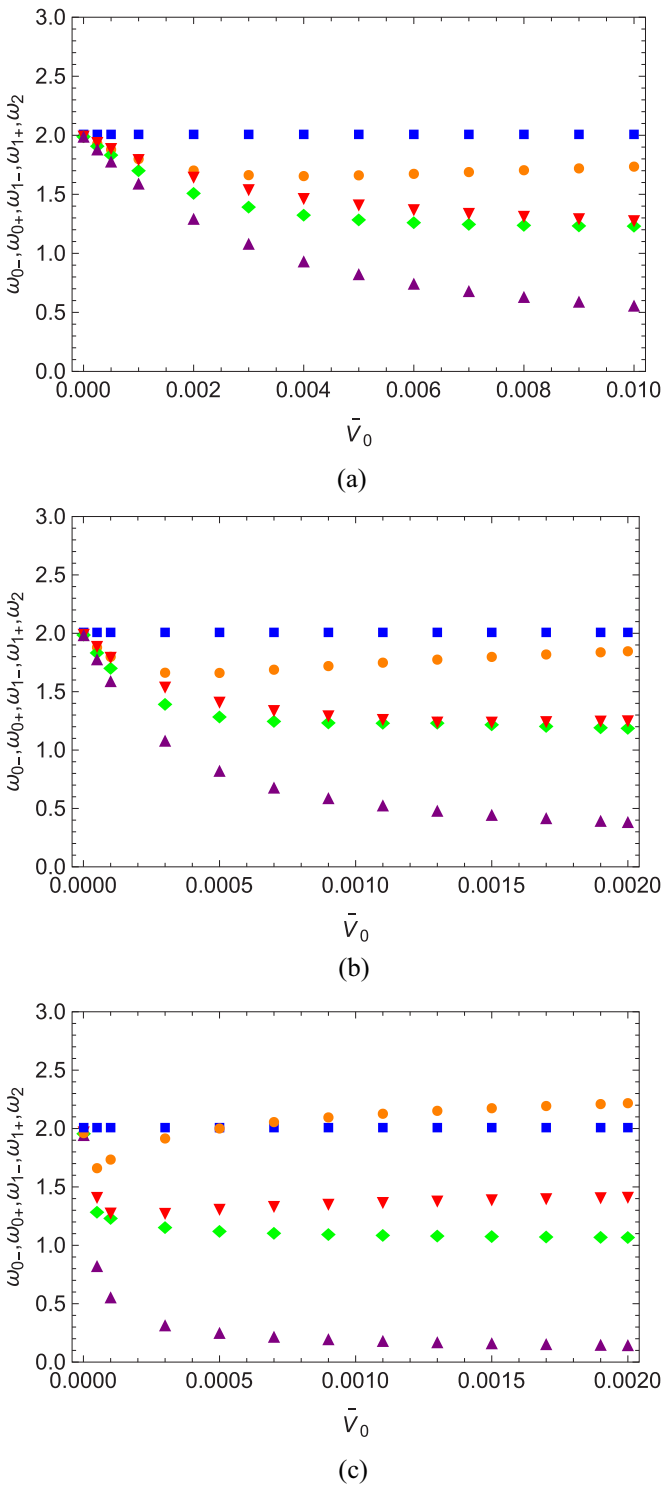

FIG. 3. Expanded view of Figs. 2(a)–2(c) near the independent-particle region, i.e., in the deep BCS regime, showing the rapid change in the frequencies when interactions turn on (ω_{0^-}, orange circles; ω_{0^+}, blue squares; ω_{1^-}, red down triangles; ω_{1^+}, green diamonds; and ω_2, purple up triangles), for (a) $N = 10^3$ fermions, (b) $N = 10^4$ fermions, and (c) $N = 10^5$ fermions. Note the small linear scale on the x axis.

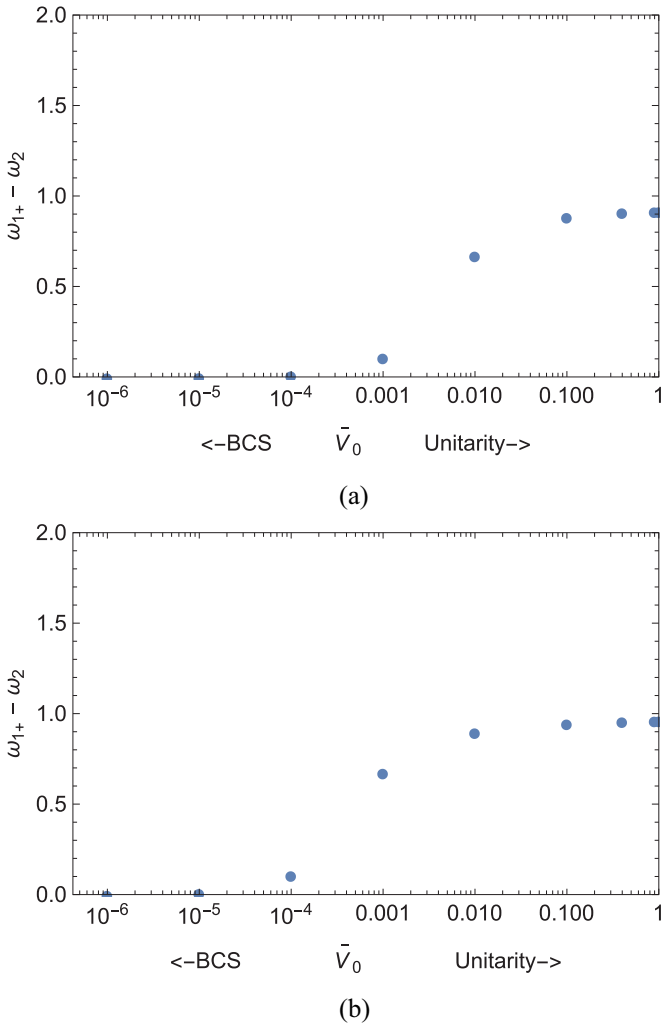

FIG. 4. Excitation gap in units of the trap frequency from the two lowest normal mode frequencies as a function of the interparticle interaction strength $\bar{V}_0$ from BCS to unitarity for (a) $N = 10^3$ fermions and (b) $N = 10^4$ fermions.

next lowest frequency, which is a particle-hole excitation, i.e., a single-particle excitation. Both of these are angular frequencies which reach stable limits, not changing as $\bar{V}_0$ increases. This particular excitation gap is relevant to the emergence and sustainability of superfluidity and is shown in Figs. 4(a) and 4(b) for system sizes of $N = 10^3$ and $N = 10^4$ particles, respectively. Note this gap emerges at lower $\bar{V}_0$, i.e., for weaker interactions for larger ensemble sizes.

In the expanded view of the region near the independent-particle limit [Figs. 3(a)–3(c)] when the interactions have just turned on, two phenomena are noticeable. First the change in the frequencies is quite rapid as soon as the interactions turn on (note the small scale on the x axis), quickly approaching values that will stabilize or change very slowly as the interactions increase. Second the frequencies separate more quickly for larger systems, i.e., as more and more particles are responding to a particular interaction strength. Thus, increasing the interaction between a fixed number of particles or increasing the number of particles experiencing a fixed interaction has a similar effect in separating the frequencies quickly. (See Sec. VI D for a discussion of the microscopic dynamics underpinning these two approaches and Appendix G for details of the analytic derivation of this effect).

B. Stable limits for angular frequencies as a function of $\bar{V}_0$

The angular frequencies evolve from the independent-particle limit to stable limits at unitarity as $\bar{V}_0$ increases. I will discuss both these limits in this section, deriving them from the analytic expressions for the frequencies in Appendixes F and G, respectively. Then, in Sec. VI, I will take advantage of the analytic forms for both the normal mode frequencies and the corresponding normal coordinates to understand the microscopic dynamics underpinning the stability of these limits by tracking the evolution of behavior including the normal mode motions of individual particles as $\bar{V}_0$ increases.

Independent-particle limit $\bar{V}_0 = 0$. Determining the values of the five frequencies is straightforward in the limit of no interactions between the particles. Setting $\bar{V}_0$ equal to zero in the transcendental equations for γ_∞ and $\bar{r}_\infty$ [see Eqs. (12)–(14)] results in values of $\gamma_\infty = 0$ and $\bar{r}_\infty = 1/\sqrt{2}$. Using these values in the formulas for the frequencies (see Appendix F) yields a value of $2\bar{\omega}_{\rm ho}$, an integer multiple of the trap frequency, as expected [4,63,64] for each of the five frequencies since the only potential affecting the particles is the harmonic trap. The individual fermions obey Fermi-Dirac statistics, but have no interactions with the other fermions in the trap. Thus all five frequencies coalesce to the same value. This can be clearly seen in Figs. 2(a)–2(c) and in the expanded view in Figs. 3(a)–3(c).

Unitary limit $\bar{V}_0 = 1.0$. As $\bar{V}_0$ is turned on and the particles begin to interact, the frequencies spread apart. The radial frequencies $\bar{\omega}_{0^-}$ and $\bar{\omega}_{1^-}$ increase while the angular frequencies evolve to limits of $\bar{\omega}_{0^+} = 2\bar{\omega}_{\rm ho}$, $\bar{\omega}_{1^+} = \bar{\omega}_{\rm ho}$, and $\bar{\omega}_2 = O(10^{-2})\bar{\omega}_{\rm ho}$. These limits for the angular frequencies are stabilized at lower values of the interaction strength for larger values of N as previously discussed and as shown in Figs. 2(a)–2(c). In Figs. 5(a) and 5(b) the approach to the unitary regime on a linear scale shows the stability of the angular frequencies and the gradual change in the radial frequencies. As will be demonstrated in the next section, the stable limits for the angular frequencies as $\bar{V}_0$ increases signify the vanishing of the interparticle interactions for these angular motions. A derivation of these limits from the analytic expressions for the angular frequencies is given in Appendix G. In the following section, the microscopic behavior that underpins this stability is analyzed using the analytic expressions for the angular frequencies and the motions as analyzed in detail in Ref. [30].

VI. UNDERSTANDING THE MICROSCOPIC DYNAMICS THAT RESULT IN STABLE LIMITS FOR THE ANGULAR FREQUENCIES

The behavior of the angular frequencies as shown in Figs. 2(a)–2(c) and discussed in the previous sections has revealed three interesting phenomena.

(1) First, the angular frequencies are evolving to stable limits independent of interactions as $\bar{V}_0$ increases while the radial frequencies continue to slowly change.

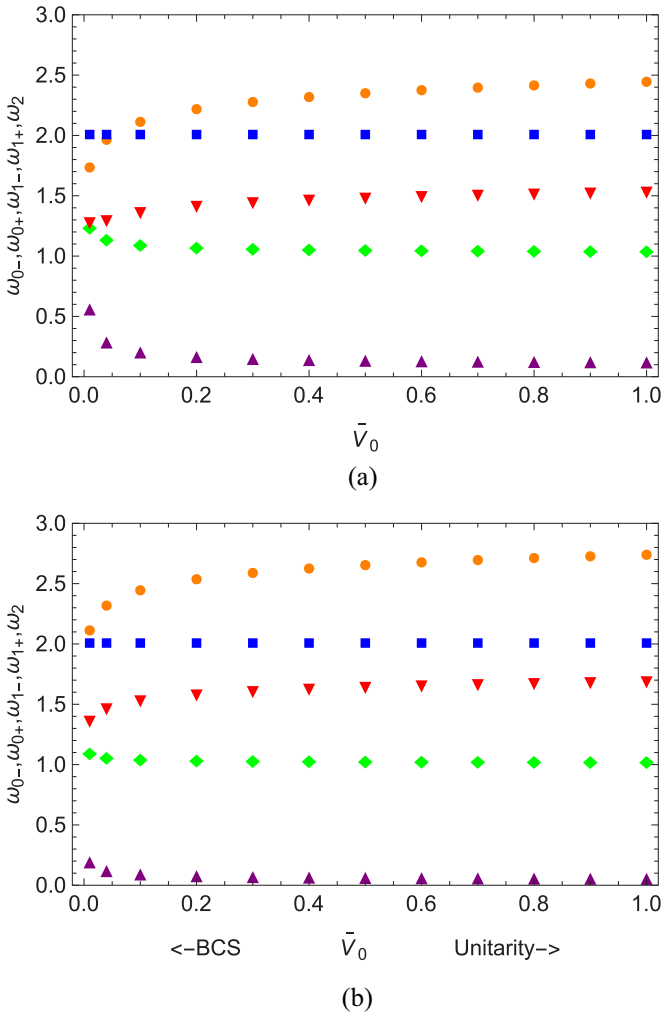

(b)

FIG. 5. Expanded view of Figs. 2(a) and 2(b) as unitarity is approached, showing the stability of the angular frequencies $\bar{\omega}_{0+}$, $\bar{\omega}_{1+}$, and $\bar{\omega}_2$ and the gradual change of the radial frequencies $\bar{\omega}_{0-}$ and $\bar{\omega}_{1-}$ (ω_{0-}, orange circles; ω_{0+}, blue squares; ω_{1-}, red down triangles; ω_{1+}, green diamonds; and ω_2, purple up triangles) for (a) $N = 10^3$ fermions and (b) $N = 10^4$ fermions.

(2) Second, the limits for the angular frequencies are integer multiples of the trap frequency.

(3) Third, the gap between the frequencies emerges at weaker interaction strengths for larger values of N.

I will now analyze the origins of these three interrelated phenomena for each of the three angular frequencies by first looking at the analytic expressions for the frequencies in these limits, then tracking the increase in correlation using the variable γ_∞, and finally analyzing the corresponding motion of the associated normal mode using the analysis in Ref. [30]. The motion of the individual particles offers an understanding of the microscopic dynamics responsible for these phenomena, including the emergence, growth, and stability of the excitation gaps as $\bar{V}_0$ increases.

Tracking contributions of terms in the Hamiltonian to analytic expressions for angular frequencies. It is enlightening to analyze the evolution of the various terms in the Hamiltonian as they contribute to the value of the frequencies as $\bar{V}_0$ increases. I will focus on terms in the effective potential which is composed of three terms, i.e., the centrifugal term that originates in the kinetic energy, the trap potential, and the interparticle potential, and focus on their effect on the angular frequencies that are relevant to the emergence of superfluid behavior in ultracold regimes. The trap potential affects all the frequencies of course, the two radial frequencies explicitly and the angular frequencies implicitly through other variables. If there are no interparticle interactions, all the frequencies would of course be integer multiples of the trap frequencies.

The analysis in Appendixes C–E shows that $\bar{V}_0$ contributes at first order to the radial frequencies [see Eqs. (C5) and (D4)], while canceling out of the expressions for the angular frequencies at first order which are dominated by the centrifugal potential terms. The remaining explicit dependence on $\bar{V}_0$ (in F_g) for the angular frequencies is small, damped by a factor of $1/N$. However, there are implicit dependences on $\bar{V}_0$ through the variables $\bar{r}_\infty$, γ_∞, $\tanh\Theta_\infty$, and $\mathrm{sech}^2\Theta_\infty$. Of these four variables, two of the variables $\tanh\Theta_\infty$ and $\mathrm{sech}^2\Theta_\infty$ play a role only in these damped terms.

Of the two remaining variables $\bar{r}_\infty$ and γ_∞, the most interesting variable to study is γ_∞, the angle cosine of each pair of particles in the large dimension maximally symmetric configuration. This variable was identified in early dimensional scaling work to signify the existence of correlation between the particles [34,45,65]. The term *correlation energy* has been defined, for example, by comparing the energies obtained in configuration-interaction calculations with Hartree-Fock mean-field energies. The correlation energy reflects the change in energy as the particles in the system move in a correlated way, thus minimizing their interactions. These early studies compared dimensional scaling results to Hartree-Fock mean-field results and noted that $\gamma_\infty = 0$ in the Hartree-Fock approximation, which is an independent-particle approximation. The nonzero values of γ_∞ at zeroth order in the dimensional expansion thus indicated that some correlation effects were being included even at lowest order, underpinning the excellent results obtained by this early work at low order [55–57].

Tracking the magnitude of γ_∞. Tracking the magnitude of γ_∞, which is a negative quantity, as $\bar{V}_0$ increases and its effect on the different terms in the expression for the frequencies has the potential to reveal insight into how the ensemble is adjusting microscopically to the introduction of interactions between the particles, specifically how the particles are rearranging from "independent" motion to collective coherent motion as correlation sets in. The Pauli principle is of course in effect as this transition occurs. Its role is fundamental, and will require an in depth study in the future. Each expression for the three angular frequencies involves several terms that involve γ_∞ from the F and G elements as seen in Eqs. (C6), (D5), (E2), and (G1)–(G3). These terms evolve as correlation increases and the magnitude of γ_∞ increases, changing the relative contributions of the kinetic energy, the trap, and the interparticle interaction to the frequency. I will analyze the response of each angular frequency to these changes in γ_∞ as correlation increases below.

Analyzing the microscopic motions of angular normal modes as unitarity is approached. What are the microscopic dynamics that are controlling this evolution to stable large

gaps at unitarity? My analysis of the motions of the normal modes in a recent study [30] makes it possible to understand the dynamics at a microscopic level as the ensemble rearranges its motion from the independent-particle case to correlated collective behavior. This motion is determined by fairly simple analytic expressions [see Eqs. (19)–(25) in Ref. [30]] that involve an intricate balancing of Kronecker δ functions and Heaviside functions that give zero or unity depending on the integer indices that refer to specific particles. This accounting keeps track of the interplay of all the particles, one by one, and offers a microscopic view of the dynamics leading to unitarity.

A. Center-of-mass frequency $\bar{\omega}_{0^+}$

The center-of-mass frequency is too large to be relevant for the emergence and support of superfluidity of ultracold gases. However, it is helpful to analyze its simple motion and well-known independence from interparticle interactions to gain insight into the dynamics of the other angular normal modes.

Independent of $\bar{V}_0$. The center-of-mass frequency is independent of interparticle interactions. The system of particles moves as a rigid body, all particles moving in lockstep with identical motions. This frequency separates out as a constant value in all the figures at twice the trap frequency for all values of N and $\bar{V}_0$. The analytic formula for $\bar{\omega}_{0^+}$ from the solution of the first-order Hamiltonian is analyzed in Appendix C and reveals the cancellation of the terms involving $\bar{V}_0$ to first order yielding an analytic expression that is insensitive to changes in the interparticle interaction strength.

Independent of N. The center-of-mass frequency is also constant as the system size increases. This is expected since a system that is independent of interparticle interactions should behave like the independent-particle case with all particles responding only to the trap, not to other interactions. Thus adding particles has no effect on the interactions experienced by the other particles and thus no effect on the frequencies. (The fermions of course obey the Pauli principle, which affects the properties of the ensemble through Fermi-Dirac statistics but does not affect the frequencies).

Microscopic dynamics. The individual particles in the center-of-mass normal mode can be seen from my analysis of the normal mode motions in Ref. [30], Secs. 3.2 and 5.1, to be executing identical very small angular motions as a rigid body with negligible change in their radial interparticle distances. Thus, these particles are not affected by the interparticle interaction resulting in a frequency that is an integer multiple (equal to 2) of the trap frequency since the trap is the only potential affecting the particles.

Response of $\bar{\omega}_{0^+}$ *to changes in* γ_∞. The center-of-mass frequency remains at a fixed value of $\bar{\omega}_{0^+} = 2\bar{\omega}_{\rm ho}$ as the variables in the analytic expression

$$\bar{\omega}_{0^+} \approx \sqrt{[G_g + 2(N-2)G_h]} \times \sqrt{F_g + 2(N-2)F_h + \frac{(N-2)(N-3)}{2}F_l} \qquad (30)$$

change in response to system parameters. How does this expression remain fixed as its various terms are changing?

Consider the independent-particle limit where $\bar{V}_0 = 0$, $\gamma_\infty = 0$, $\bar{r}_\infty = 1/\sqrt{2}$, and the particles are affected only by the harmonic trap while obeying the Pauli principle. Most of the terms in the expression for $\bar{\omega}_{0^+}$ are zero. The only nonzero terms are G_g and F_g (see Appendix F), which both originate in the kinetic energy, depend implicitly on the trap potential, and involve a dependence on just two particles i and j through the variable γ_{ij}. As $\bar{V}_0$ turns on, γ_∞ takes on a small nonzero value, signifying that weak correlations exist. This nonzero value now means that all of the terms in $\bar{\omega}_{0^+}$ are nonzero and G_g and F_g evolve to new values. Specifically, G_h, F_h, and F_i acquire nonzero values and involve the dependence of the kinetic energy (G_h) and the centrifugal potential (F_h and F_i) on $\gamma_{ij}\gamma_{jk}$, i.e., involving three particles i, j, and k, and on $\gamma_{ij}\gamma_{kl}$, involving four particles i, j, k, and l. These terms become significant in determining the value of the frequency with factors of $2(N-2)$ for F_h and $(N-2)(N-3)/2$ for F_i as interparticle correlations increase. Since the value of $\bar{\omega}_{0^+}$ remains fixed at 2, the magnitudes of G_g and F_g adjust as correlations spread throughout the ensemble. Thus, the emergence of interparticle interactions starts an intricate readjustment of the ensemble as the particles governed by the evolving Hamiltonian respond to the other $N-1$ particles.

B. Angular particle-hole excitation frequency $\bar{\omega}_{1^+}$

Now consider the angular single-particle excitation frequency $\bar{\omega}_{1^+}$, which can also be described as a particle-hole angular excitation.

Independent of $\bar{V}_0$. This frequency reaches a constant value equal to the trap frequency as $\bar{V}_0$ increases, reflecting the vanishing of interparticle interactions. The analytic formula for $\bar{\omega}_{1^+}$ analyzed in Appendix D reveals the cancellation of the terms involving $\bar{V}_0$ to first order. Thus this frequency is expected to become constant as the interaction changes if higher-order terms are small.

Independent of N. It also becomes constant as the system size increases since the frequency is insensitive to all interparticle interactions so additional particles have no effect.

Microscopic dynamics. This behavior can be understood from a microscopic view of the motions of the particles. In this case, the motion of the corresponding normal mode is made up of one particle creating a "large" angular displacement with the other particles, while the remaining interparticle angles make a small adjustment. The first group has $N-1$ interparticle angles, while the second group of $(N-1)(N-2)/2$ angles quickly becomes the overwhelming majority of the ensemble with displacements that are smaller by a factor of $(N-2)/2$. (See Secs. 3.4 and 5.1 in Ref. [30]). These two opposing and unequal motions invoke some radial interactions from slight changes in the interparticle distances and thus this mode does have some response to the interaction $\bar{V}_0$. However, for values of N typical of laboratory ensembles (10^4–10^6), the percentage of particles moving in lockstep by a smaller and smaller angular amount becomes so dominant that the radial contribution is insignificant. Thus the harmonic trap is the dominant effect determining this frequency, analogous to the center-of-mass frequency. This explains the value of the frequency at an integer multiple (equal to 1) of the trap frequency and its independence from changes in $\bar{V}_0$ and/or N.

Response of $\bar{\omega}_{1^+}$ to changes in γ_∞. When $\bar{V}_0 = 0$ and the particles are moving independently, $\gamma_\infty = 0$ and $\bar{r}_\infty = 1/\sqrt{2}$, only G_g and F_g in the expression for $\bar{\omega}_{1^+}$ are nonzero with values determined by the harmonic trap yielding $2\bar{\omega}_{\rm ho}$, a integer multiple of the trap frequency for $\bar{\omega}_{1^+}$ (see Appendix F),

$$\begin{aligned}\bar{\omega}_{1^+} &\approx \sqrt{G_g + (N-4)G_h} \\ &\quad \times \sqrt{F_g + (N-4)F_h - (N-3)F_i} \\ &\rightarrow 2\bar{\omega}_{\rm ho} \quad (G_g = 4,\ F_g = 1,\ G_h = F_h = F_i = 0). \quad (31)\end{aligned}$$

As interparticle interactions are introduced, γ_∞ is no longer zero, so G_h, F_h, and F_i contribute as interparticle correlations increase. Smaller factors for F_h of $(N-4)$ and a negative factor of $-(N-3)$ for F_i result in a smaller value of $\bar{\omega}_{1^+}$ which evolves to $\bar{\omega}_{\rm ho}$ from its value of $2\bar{\omega}_{\rm ho}$ at the independent particle limit. The magnitudes of G_g and F_g adjust as the changing value of γ_∞ signifies longer-range correlations introducing new contributions involving three and four particles.

C. Phonon frequency $\bar{\omega}_2$

Finally consider the angular phonon compressional frequency $\bar{\omega}_2$. This frequency reaches a constant value that is two or three orders of magnitude smaller than the trap frequency as $\bar{V}_0$ increases.

Independent of $\bar{V}_0$. The analytic formula for $\bar{\omega}_2$,

$$\bar{\omega}_2 = \sqrt{[G_g - 2G_h][F_g - 2F_h + F_i]},$$

analyzed in Appendix E, reveals the insignificance of the terms involving $\bar{V}_0$ to first order. Thus this frequency is expected to become constant as the interaction increases.

Independent of N. It also becomes constant as the system size increases since adding particles has no effect on this frequency, which is independent of the interparticle interaction to first order.

Microscopic dynamics. In this third case, the motion of the corresponding normal mode is made up of three groups of interparticle angles involving particles that move with different angular motions and amounts: a single dominant interparticle angle which has the largest angular displacement, $2(N-2)$ nearest-neighbor angles which move with an opposing angular displacement that is smaller than that of the dominant angle by a factor of $(N-2)$, and a third group which quickly becomes the dominant group of particles involving $(N-2)(N-3)/2$ angles which have a displacement that is a factor of $(N-2)(N-3)/2$ smaller than the dominant angle. (See Secs. 3.5 and 5.1– 5.1.3 in Ref. [30]). These groups move in opposing directions with unequal displacements and thus experience some radial interparticle interactions. However, as N increases, the percentage of particles moving in lockstep in the third group by a smaller and smaller angular amount becomes so dominant that the radial contribution due to the movement of the other two groups is negligible. (See Sec. 5.1.3 in Ref. [30]). This results in the value of the frequency at an integer multiple (approximately equal to 0) of the trap frequency and independence from changes in $\bar{V}_0$ and/or N.

Response of $\bar{\omega}_2$ to changes in γ_∞. When $\bar{V}_0 = 0$ and the particles are moving independently affected only by the trap potential, $\gamma_\infty = 0$ and $\bar{r}_\infty = 1/\sqrt{2}$. The nonzero terms G_g and F_g depend on γ_{ij} (see Appendix F). As $\bar{V}_0$ turns on, γ_∞ is nonzero, so all terms in $\bar{\omega}_2$ are now nonzero and involve a dependence on $\gamma_{ij}\gamma_{jk}$ and $\gamma_{ij}\gamma_{kl}$. Since the value of $\bar{\omega}_2$ evolves to very small values from $2\bar{\omega}_{\rm ho}$, the magnitudes of G_g and F_g must adjust as longer-range correlations throughout the ensemble reflect the realignment of the particles into collective motion.

D. Discussion of the microscopic dynamics

The dynamics that drive the angular frequencies to integer multiples of the trap frequency at unitarity are responsible for both the large excitation gap between the two lowest normal modes and the independence of the ensemble from the microscopic interaction, details consistent with the expected universal behavior. There are in fact two distinct dynamical effects that can produce this behavior. The discussion of the microscopic dynamics in the above paragraphs assumes large values of N typical of experiments with ultracold Fermi gases to understand these stable limits as the interparticle interactions vanish. However, increasing $\bar{V}_0$ can also result in the angular frequencies approaching integer multiples of the trap frequency for fixed values of N. These two effects can be seen in the figures in Sec. V, which show $\bar{V}_0$ increasing for several fixed ensemble sizes. This complementary behavior as either N or $\bar{V}_0$ increases was previously noted at the end of Sec. V A and an analytic derivation of these two effects is given in Appendix G. I discuss both these behaviors in more detail below.

Two distinct microscopic dynamics. As discussed above, when N increases to large values, the percentage of particles that have very small angular movements, i.e., $\gamma_{ij} \ll 1$ in the $[N-1, 1]$ and $[N-2, 2]$ angular modes, becomes the overwhelming majority of particles in the ensemble. (The center-of-mass mode of course has all the particles moving in lockstep with amounts that are small when N is large). The angular motion, i.e., the magnitude of γ_{ij}, for this majority of particles becomes smaller and smaller as N increases. (See Sec. 5.1 in Ref. [30]). Since purely angular motions produce no change in the radial distances from the center of the trap, i.e., $\bar{r}_i$ and $\bar{r}_j$ are constant, this motion yields negligible changes in the interparticle distances $\bar{r}_{ij} = \sqrt{\bar{r}_i^2 + \bar{r}_j^2 - 2\bar{r}_i\bar{r}_j\gamma_{ij}}$ when γ_{ij} is tiny.

Now consider letting $\bar{V}_0$ increase for fixed system size. The correlation between the particles increases as tracked by the parameter γ_∞. This happens quite rapidly as $\bar{V}_0$ increases from zero, reflecting the rearrangement of the particles into correlated angular motion as collective behavior sets in. This dynamic is relevant to experiments using Feshbach resonances to tune interactions to the large values of the unitary regime. As correlations spread throughout the ensemble into this rigid angular motion, the interparticle interactions become negligible for this fixed value of N and the system is independent of the details of the microscopic interactions.

Microscopic dynamics of unitarity. The two lowest normal modes in the unitary regime have frequencies that set up an excitation gap that is stable and independent of the microscopic details of the interaction. The spectrum of the $[N-1, 1]$ angular mode has evenly spaced levels at every

integer multiple of the trap frequency, identical to the spectrum of the noninteracting regime of independent particles. The strong interactions of the unitary regime result in synchronized correlated behavior that paradoxically have minimal interparticle interactions.

The unitarity limit is defined as having no interaction length scale due to strong interactions that are much shorter range than the interparticle distance, leaving the oscillator length and the interatomic distance as the only relevant length scales. The interatomic distance is the defining characteristic of an angular normal mode which has all (center-of-mass mode) or the overwhelming majority (angular particle-hole excitation and phonon modes) of the particles moving as a rigid body with collisionless motion. The gas is expected to show a universal thermodynamic behavior at zero temperature, independent of any microscopic details of the underlying interactions.

VII. CONCLUSION

In this study, I have looked in detail at the analytic frequencies for N identical particles as a function of the interparticle interaction strength as it is tuned from weakly interacting regimes to the strong interactions of the unitary regime. The frequencies were obtained previously from the normal mode solutions to the SPT first-order equation in inverse dimensionality for a system of confined, interacting, identical particles. These N-body normal modes were determined analytically as a function of various system parameters and used to construct wave functions and density profiles for systems of identical bosons [32,34,35] and later energies [38] and thermodynamic quantities for fermions [40,41].

The present investigation was motivated by a recent study of the evolution of the N-body analytic-normal-mode coordinates as N increases from few-body systems that have good molecular equivalents to the expected behavior of many-body ensembles [30]. A specific Hamiltonian, that of the unitary regime, was investigated and two phenomena were noted that could sustain the emergence and stability of superfluid behavior. In this paper, I have extended the study of these two phenomena to a range of interaction strengths from BCS to unitarity.

In particular, I have investigated closely the behavior of the two lowest angular frequencies, a single-particle angular excitation and a compressional phonon mode, that are relevant to the emergence of excitation gaps that could support superfluidity. I used both the analytic expressions for the frequencies, which allow the different contributions from Hamiltonian terms to be assessed, and the simple analytic expressions for the normal mode motions [30] to gain insight into the microscopic dynamics underpinning this evolution. The single-particle angular excitation is a particle-hole excitation, i.e., a rearrangement of the particles within the ensemble due to the angular excitation of a single particle creating a hole, not the loss of a particle due to angular motion. The low-frequency phonon mode, while similar to the long-wavelength compressional modes appearing in other formalisms such as Goldstone modes [66–68] and Bogoliubov-Anderson phonons [68–71], is distinct from these modes since it is not composed of Cooper pairs. The phonon mode in the SPT formalism is a normal mode function providing a coherent macroscopic wave function with many-body pairing.

Summary. In summary, my analysis has resulted in a number of observations that may prove useful in understanding the emergence, growth, and stability of excitation gaps as well as offering a possible explanation of the microscopic dynamics responsible for universal behavior at unitarity. I list them below.

(1) The analytic expressions for the normal mode frequencies produce behavior that supports the emergence of excitation gaps consistent with the known behavior of ultracold Fermi gases in the laboratory tuned using Feshbach resonances from the weakly interacting BCS regime with small gaps to the large gaps of the strongly interacting unitary regime.

(2) The normal modes evolve to almost purely radial or purely angular character as N increases, with very little mixing of the symmetry coordinates, over the entire transition from BCS to unitarity. This confirms that the frequencies can be labeled as radial or angular and affects the stability since the symmetry coordinates are analytic solutions of an underlying approximate Hamiltonian.

(3) As $\bar{V}_0$ increases from zero at the independent-particle limit, these first-order analytic frequencies rapidly separate. As unitarity is approached the angular frequencies stabilize while the radial frequencies continue to slowly change. This suggests that higher-order terms may be necessary to converge the radial frequencies.

(4) The change in the frequencies emerges at weaker interaction strengths as the ensemble grows. Thus, increasing the number of particles experiencing a fixed interaction or increasing the interaction between a fixed number of particles has a similar effect in separating the frequencies quickly.

(5) The largest gap forms between the extremely-low-frequency angular phonon mode, which is the only mode occupied by ultracold gases, and the next lowest frequency, which is an angular particle-hole excitation, i.e., a single-particle excitation. This particular excitation gap is relevant to the emergence and sustainability of superfluidity in ultracold systems.

(6) The limits for the three angular frequencies are integer multiples of the trap frequency, reflecting the interaction independence of these frequencies.

(7) The two lowest normal mode frequencies relevant to ultracold gases provide a spectrum of evenly spaced levels at integer multiples of the trap frequency at unitarity, identical to the spectrum of the noninteracting regime of independent particles. This spectrum is of course independent of any microscopic details of the underlying interactions consistent with the dynamics expected for the unitary regime. Thus, the strong interactions of the unitary regime result in strong long-range correlated behavior that paradoxically has minimal interparticle interactions.

(8) Two distinct dynamical effects were found that can drive the angular frequencies to integer multiples of the trap frequency at unitarity. First, when N increases, the angular phonon and single-particle excitation modes that are involved in creating an excitation gap for ultracold particles now have an overwhelming percentage of particles moving with small purely angular motions that have a negligible response to

interparticle interactions. This results in angular frequencies at integer multiples of the trap frequency since the trap is the only potential affecting the particles. Second, as $\bar{V}_0$ increases for fixed N, correlations increase and become long range as tracked by the parameter γ_∞. The motion evolves into rigid angular motion as interparticle interactions vanish, yielding frequencies at integer multiples of the trap frequency.

Conclusions. This analysis of the normal mode frequencies yields consistent, physically intuitive behavior that has been observed in the laboratory. The microscopic dynamics underlying this behavior are based on normal mode motions and thus are different from the accepted view that the relevant particles in a superfluid form loosely bound pairs that decrease in size as a Feshbach resonance is tuned to strong interactions.

Normal modes have an infinite spectrum of evenly spaced excited states. At unitarity, the spectrum involved in an excitation gap for ultracold fermions consists of integer steps of the trap frequency identical to the spectrum of the noninteracting independent-particle limit. This behavior supports dynamics at unitarity that are independent of interparticle interactions. Despite having the same spectrum, the dynamics of independent fermions in a trap are quite different from the dynamics of fermions at unitarity whose behavior reflects the strong interactions that have been encapsulated into normal mode motions. A full understanding of how this spectrum affects the dynamics at unitarity requires an understanding of the role of the Pauli principle which is a subject left for future study.

If higher-order effects are small, the normal coordinates whose frequencies and mixing coefficients depend on the interparticle interactions are in fact beyond-mean-field analytic solutions to a many-body Hamiltonian. The frequencies and the motions of the normal modes evolve in sync with each other, both responding to the same microscopic dynamics. These analytic forms for the frequencies and coordinates allow the details of the terms in the Hamiltonian that are driving the dynamics to be revealed in a particularly transparent way.

Specifically, I looked at the change in the parameter γ_∞ whose magnitude increases as $\bar{V}_0$ increases, signaling an increase in the strength and long-range character of correlation as terms involving three and four particles begin to contribute to the values of the frequencies.

The dynamics revealed by this study are based on a exact solution of the first-order equation of SPT. If higher-order terms are significant in a particular regime along this transition, the dynamics could change. In particular, the radial frequencies (which are not involved in providing excitation gaps for ultracold gases) do not show stable limits as unitarity is approached, which suggests that higher-order terms are needed for these frequencies. First-order SPT results have been tested only in the unitary regime, i.e., for strong interactions, yielding ground-state energies comparable to benchmark Monte Carlo results [38] and excellent agreement with experiment for thermodynamic quantities [41]. The weakly interacting regime has so far been unexplored using this formalism. This approach also does not offer an efficient mechanism for the two-body pairing in real space that occurs beyond unitarity as the ensemble transitions to the BEC regime.

Normal mode functions provide simple, coherent macroscopic wave functions with phase coherence over the entire system. The dynamics of a normal mode description of the BCS to unitarity transition with its many-body pairing offer an interesting alternative to the models relying on two-body pairing mechanisms to achieve superfluidity. This approach also offers a possible microscopic understanding of the universal behavior at unitarity which could be applicable to other strongly correlated superfluids in diverse systems.

ACKNOWLEDGMENT

I am grateful to the National Science Foundation for financial support through Grants No. PHY-1607544 and No. PHY-2011384.

APPENDIX A: MIXING COEFFICIENTS FOR THE [N] AND [$N-1, 1$] SECTORS

The mixing coefficients for the [N] sector are

$$\cos\theta_+^{[N]} = \frac{\sqrt{2}\sqrt{N-1}[c+(N/2-1)d]}{\sqrt{2(N-1)[c+(N/2-1)d]^2+[-a-(N-1)b+\lambda_{[N]}^+]^2}}, \tag{A1}$$

$$\sin\theta_+^{[N]} = \frac{-a-(N-1)b+\lambda_{[N]}^+}{\sqrt{2(N-1)[c+(N/2-1)d]^2+[-a-(N-1)b+\lambda_{[N]}^+]^2}}, \tag{A2}$$

$$\cos\theta_-^{[N]} = \frac{\sqrt{2}\sqrt{N-1}[c+(N/2-1)d]}{\sqrt{2(N-1)[c+(N/2-1)d]^2+[-a-(N-1)b+\lambda_{[N]}^-]^2}}, \tag{A3}$$

$$\sin\theta_-^{[N]} = \frac{-a-(N-1)b+\lambda_{[N]}^-}{\sqrt{2(N-1)[c+(N/2-1)d]^2+[-a-(N-1)b+\lambda_{[N]}^-]^2}}, \tag{A4}$$

while the coefficients in the [$N-1, 1$] sector are

$$\cos\theta_+^{[N-1,1]} = \frac{\sqrt{N-2}(c-d)}{\sqrt{(N-2)(c-d)^2+(-a+b+\lambda_{[N-1,1]}^+)^2}}, \tag{A5}$$

$$\sin\theta_+^{[N-1,1]} = \frac{-a+b+\lambda_{[N-1,1]}^+}{\sqrt{(N-2)(c-d)^2+(-a+b+\lambda_{[N-1,1]}^+)^2}}, \tag{A6}$$

$$\cos\theta_{-}^{[N-1,1]} = \frac{\sqrt{N-2}(c-d)}{\sqrt{(N-2)(c-d)^2 + (-a+b+\lambda_{[N-1,1]}^{-})^2}}, \tag{A7}$$

$$\sin\theta_{-}^{[N-1,1]} = \frac{-a+b+\lambda_{[N-1,1]}^{-}}{\sqrt{(N-2)(c-d)^2 + (-a+b+\lambda_{[N-1,1]}^{-})^2}}, \tag{A8}$$

where $\lambda_{[N]}^{\pm}$ and $\lambda_{[N-1,1]}^{\pm}$ are given by Eqs. (24)–(28) in Sec. IV. The above equations have some explicit N dependence (but no $\bar{V}_0$ dependence) that is due to the symmetry present in the first-order Hamiltonian. The quantities a, b, c, d, e, f, g, h, and i in the expressions for the mixing coefficients and the eigenvalues $\lambda_{[N]}^{\pm}$ and $\lambda_{[N-1,1]}^{\pm}$ are defined in Appendix B [see also Eq. (42) in Ref. [31]] in terms of the F and G elements and have explicit N and $\bar{V}_0$ dependence as well as N and $\bar{V}_0$ dependence from the F and G elements from a particular Hamiltonian. Thus there are three layers of analytic expressions that can introduce N and/or $\bar{V}_0$ dependence: the expressions for mixing coefficients in Eqs. (A1)–(A8) above, the expressions for a, b, c, d, e, f, g, h, ι, $\lambda_{[N]}^{\pm}$, and $\lambda_{[N-1,1]}^{\pm}$, and the expressions for the F and G elements for a specific Hamiltonian.

APPENDIX B: THE *FG* MATRIX ELEMENTS

The constants used in the expressions for the mixing coefficients and the frequencies are defined below:

$$\begin{aligned}
a &= G_a F_a,\\
b &= G_a F_b,\\
c &= G_g F_e + (N-2) G_h (F_e + F_f),\\
d &= G_g F_f + 2 G_h [F_e + (N-3) F_f],\\
e &= G_a F_e,\\
f &= G_a F_f,\\
g &= G_g F_g + 2(N-2) G_h F_h,\\
h &= G_g F_h + G_h F_g + (N-2) G_h F_h + (N-3) G_h F_\iota,\\
\iota &= G_g F_\iota + 4 G_h F_h + 2(N-4) G_h F_\iota.
\end{aligned} \tag{B1}$$

The nonzero elements of the $\boldsymbol{G}$ matrix are

$$\begin{aligned}
G_a &= G_{\bar{r}_i \bar{r}_i} = 1,\\
G_g &= G_{\gamma_{ij}\gamma_{ij}} = 2\frac{1-{\gamma_\infty}^2}{\bar{r}_\infty^2} = 4[1+(N-1)\gamma_\infty](1+\gamma_\infty)(1-\gamma_\infty),\\
G_h &= G_{\gamma_{ij}\gamma_{jk}} = \frac{\gamma_\infty(1-\gamma_\infty)}{\bar{r}_\infty^2} = 2[1+(N-1)\gamma_\infty]\gamma_\infty(1-\gamma_\infty),
\end{aligned}$$

where the matrix elements have been evaluated at the infinite-D symmetric minimum. Likewise, the nonzero $\boldsymbol{F}$ matrix elements are

$$\begin{aligned}
F_a &= \left(\frac{\partial^2 \bar{V}_{\rm eff}}{\partial \bar{r}_i^2}\right)\Big|_\infty\\
&= 1 + \frac{3}{4\bar{r}_\infty^4}\frac{1+(N-2)\gamma_\infty}{(1-\gamma_\infty)[1+(N-1)\gamma_\infty]} + \frac{\bar{V}_0\bar{c}_0}{2}(N-1)\operatorname{sech}^2\Theta_\infty\left[\bar{c}_0(1-\gamma_\infty)\tanh\Theta_\infty - \frac{1+\gamma_\infty}{2\bar{r}_\infty\sqrt{1-\gamma_\infty}}\right],
\end{aligned} \tag{B2}$$

$$F_b = \left(\frac{\partial^2 \bar{V}_{\rm eff}}{\partial \bar{r}_i \partial \bar{r}_j}\right)\Big|_\infty = \frac{\bar{V}_0\bar{c}_0}{2}\operatorname{sech}^2\Theta_\infty\left[\bar{c}_0(1-\gamma_\infty)\tanh\Theta_\infty + \frac{1+\gamma_\infty}{2\bar{r}_\infty\sqrt{1-\gamma_\infty}}\right],$$

$$F_e = \left(\frac{\partial^2 \bar{V}_{\rm eff}}{\partial \bar{r}_i \partial \gamma_{ij}}\right)\Big|_\infty = -\frac{\gamma_\infty}{2\bar{r}_\infty^3}\frac{1+(N-2)\gamma_\infty}{(1-\gamma_\infty)^2[1+(N-1)\gamma_\infty]^2} + \frac{\bar{V}_0\bar{c}_0}{2}\operatorname{sech}^2\Theta_\infty\left[-\bar{c}_0\bar{r}_\infty\tanh\Theta_\infty + \frac{1}{2\sqrt{1-\gamma_\infty}}\right], \tag{B3}$$

$$F_f = \left(\frac{\partial^2 \bar{V}_{\rm eff}}{\partial \bar{r}_i \partial \gamma_{jk}}\right)\Big|_\infty = \frac{\gamma_\infty^2}{2\bar{r}_\infty^3(1-\gamma_\infty)^2[1+(N-1)\gamma_\infty]^2}, \tag{B4}$$

$$\begin{aligned}
F_g &= \left(\frac{\partial^2 \bar{V}_{\rm eff}}{\partial \gamma_{ij}^2}\right)\Big|_\infty\\
&= \frac{1}{2\bar{r}_\infty^2(1-\gamma_\infty)^3[1+(N-1)\gamma_\infty]^3}\left[1+3(N-2)\gamma_\infty + (13-11N+3N^2)\gamma_\infty^2 + (N-2)(4-3N+N^2)\gamma_\infty^3\right]\\
&\quad + \frac{\bar{V}_0\bar{c}_0}{2}\operatorname{sech}^2\Theta_\infty\left[\frac{\bar{c}_0\bar{r}_\infty^2}{1-\gamma_\infty}\tanh\Theta_\infty + \frac{\bar{r}_\infty}{2(1-\gamma_\infty)^{3/2}}\right],
\end{aligned}$$

$$F_h = \left(\frac{\partial^2 \bar{V}_{\rm eff}}{\partial \gamma_{ij} \partial \gamma_{jk}}\right)\Big|_\infty = \frac{-\gamma_\infty}{4\bar{r}_\infty^2(1-\gamma_\infty)^3[1+(N-1)\gamma_\infty]^3}\left[3+(5N-14)\gamma_\infty + (11-9N+2N^2)\gamma_\infty^2\right], \tag{B5}$$

$$F_\iota = \left(\frac{\partial^2 \bar{V}_{\rm eff}}{\partial\gamma_{ij}\partial\gamma_{kl}}\right)\Bigg|_\infty = \frac{\gamma_\infty^2[2+(N-2)\gamma_\infty]}{\bar{r}_\infty^2(1-\gamma_\infty)^3[1+(N-1)\gamma_\infty]^3}. \tag{B6}$$

Inspection of the formulas for F elements easily reveals the explicit dependence of their terms on the confining (trap) potential $\bar{V}_{\rm conf}$, the centrifugal potential $\bar{U}$, and/or the interparticle interaction potential $\bar{V}_0$. All the terms also have some implicit dependence on all the terms in $\bar{V}_{\rm eff}$ through the variables $\bar{r}_\infty$ and γ_∞. I list the explicit contributions below:

$$\begin{aligned}
F_a &\Leftrightarrow \bar{V}_{\rm conf}, \bar{U}, \bar{V}_0 \text{ (strong)},\\
F_b &\Leftrightarrow \bar{V}_0 \text{ (weak)},\\
F_e &\Leftrightarrow \bar{U}, \bar{V}_0 \text{ (weak)},\\
F_f &\Leftrightarrow \bar{U},\\
F_g &\Leftrightarrow \bar{U}, \bar{V}_0 \text{ (weak)},\\
F_h &\Leftrightarrow \bar{U},\\
F_\iota &\Leftrightarrow \bar{U}.
\end{aligned}$$

Using the fact that the three nonzero G elements and the centrifugal "potential" terms originate in kinetic energy terms of the Hamiltonian, it is possible to classify the a, b, c, d, e, f, g, h, and ι terms. Since they all contain one of the three G elements, they all have a contribution from the kinetic energy. Below I list the explicit contributions in terms of the potentials:

$$\begin{aligned}
a &= G_a F_a \Leftrightarrow \bar{V}_{\rm conf}, \bar{U}, \bar{V}_0 \text{ (strong)},\\
b &= G_a F_b \Leftrightarrow \bar{V}_0 \text{ (weak)},\\
c &= G_g F_e + (N-2) G_h (F_e + F_f) \Leftrightarrow \bar{U}, \bar{V}_0 \text{ (weak)},\\
d &= G_g F_f + 2 G_h (F_e + (N-3) F_f) \Leftrightarrow \bar{U}, \bar{V}_0 \text{ (weak)},\\
e &= G_a F_e \Leftrightarrow \bar{U}, \bar{V}_0 \text{ (weak)},\\
f &= G_a F_f \Leftrightarrow \bar{U},\\
g &= G_g F_g + 2(N-2) G_h F_h \Leftrightarrow \bar{U}, \bar{V}_0 \text{ (weak)},\\
h &= G_g F_h + G_h F_g + (N-2) G_h F_h + (N-3) G_h F_\iota\\
&\quad \Leftrightarrow \bar{U}, \bar{V}_0 \text{ (weak)},\\
\iota &= G_g F_\iota + 4 G_h F_h + 2(N-4) G_h F_\iota \Leftrightarrow \bar{U}.
\end{aligned}$$

APPENDIX C: ANALYSIS OF THE [N] SECTOR FREQUENCIES

The frequencies $\bar{\omega}_{0^\pm}$ associated with the roots $\lambda_{0^\pm}$ of multiplicity 1 are given by

$$\bar{\omega}_{0^\pm} = \sqrt{\eta_0 \mp \sqrt{\eta_0^2 - \Delta_0}}, \tag{C1}$$

$$\begin{aligned}
\eta_0 &= \frac{1}{2}\Bigg[a + (N-1)b + g + 2(N-2)h\\
&\quad + \frac{(N-2)(N-3)}{2}\iota\Bigg],\\
\Delta_0 &= [a + (N-1)b]\left[g + 2(N-2)h + \frac{(N-2)(N-3)}{2}\iota\right]\\
&\quad - \frac{N-1}{2}[2c + (N-2)d][2e + (N-2)f],
\end{aligned} \tag{C2}$$

$$\begin{aligned}
\eta_0^2 - \Delta_0 &= \frac{1}{4}\Bigg[a + (N-1)b - \Bigg(g + 2(N-2)h\\
&\quad + \frac{(N-2)(N-3)}{2}\iota\Bigg)\Bigg]^2\\
&\quad + \frac{N-1}{2}[2c + (N-2)d][2e + (N-2)f].
\end{aligned} \tag{C3}$$

Defining

$$\begin{aligned}
A &= a + (N-1)b,\\
T &= g + 2(N-2)h + \frac{(N-2)(N-3)}{2}\iota
\end{aligned}$$

and substituting the definitions of a, b, c, d, e, f, g, h, and ι in terms of F and G elements yields

$$\begin{aligned}
A &= G_a F_a + (N-1) G_a F_b,\\
T &= [G_g + 2(N-2)G_h]\\
&\quad \times\left[F_g + 2(N-2)F_h + \frac{(N-2)(N-3)}{2}F_\iota\right]\\
&= T_1 T_2,\\
2c + (N-2)d &= [G_g + 2(N-2)G_h][2F_e + (N-2)F_f]\\
&= T_1 T_3,\\
2e + (N-2)f &= [2F_e + (N-2)F_f]\\
&= T_3.
\end{aligned}$$

So

$$\begin{aligned}
\bar{\omega}_{0^\pm} &= \sqrt{\eta_0 \mp \sqrt{\eta_0^2 - \Delta_0}}\\
&= \sqrt{\frac{1}{2}[A+T] \mp \sqrt{\frac{1}{4}[A-T]^2 + \frac{N-1}{2}T_1 T_3^2}}.
\end{aligned}$$

Thus,

$$\begin{aligned}
\omega_{0^-} &= \sqrt{\tfrac{1}{2}[A+T] + \tfrac{1}{2}[A-T](1+x)^{1/2}},\\
\omega_{0^+} &= \sqrt{\tfrac{1}{2}[A+T] - \tfrac{1}{2}[A-T](1+x)^{1/2}},
\end{aligned} \tag{C4}$$

where

$$x = \frac{\frac{N-1}{2}T_1 T_3^2}{\frac{1}{4}(A-T)^2}$$

is small. Thus the two frequencies $\omega_{0^\pm}$ in the [N] sector split into a frequency ω_{0^-}, which has a leading term (under the square root) A with a strong dependence on the interparticle interaction potential $\bar{V}_0$, and a frequency ω_{0^+}, in which A cancels out, leaving a leading term T that depends on the

centrifugal terms. The powers of x introduce higher-order terms

$$\omega_{0^-} \approx \sqrt{A} = \sqrt{a + (N-1)b} = \sqrt{G_a F_a + (N-1)G_a F_b}, \tag{C5}$$

$$\omega_{0^+} \approx \sqrt{T} = \sqrt{g + 2(N-2)h + \frac{(N-2)(N-3)}{2}\iota} = \sqrt{G_g + 2(N-2)G_h} \times \sqrt{F_g + 2(N-2)F_h + \frac{(N-2)(N-3)}{2}F_\iota}. \tag{C6}$$

APPENDIX D: ANALYSIS OF THE $[N-1, 1]$ SECTOR FREQUENCIES

The frequencies $\bar{\omega}_{1^\pm}$ associated with the roots $\lambda_{1^\pm}$ of multiplicity $N-1$ are given by

$$\bar{\omega}_{1^\pm} = \sqrt{\eta_1 \mp \sqrt{{\eta_1}^2 - \Delta_1}}, \tag{D1}$$

$$\eta_1 = \tfrac{1}{2}[a - b + g + (N-4)h + (N-3)\iota],$$
$$\Delta_1 = (a-b)[g + (N-4)h - (N-3)\iota] - (N-2)(c-d)(e-f), \tag{D2}$$

$$\eta_1^2 - \Delta_1 = \tfrac{1}{4}\{a - b - [g + (N-4)h - (N-3)\iota]\}^2 + (N-2)(c-d)(e-f). \tag{D3}$$

Defining

$$B = a - b,$$
$$R = g + (N-4)h - (N-3)\iota$$

and substituting the definitions of a, b, c, d, e, f, g, h, and ι in terms of F and G elements yields

$$B = G_a F_a - G_a F_b,$$
$$R = [G_g + (N-4)G_h][F_g + (N-4)F_h - (N-3)F_\iota] = R_1 R_2,$$
$$c - d = [G_g + (N-4)G_h] \times [F_e - F_f] = R_1 R_3,$$
$$e - f = [F_e - F_f] = R_3.$$

So

$$\bar{\omega}_{1^\pm} = \sqrt{\eta_1 \mp \sqrt{{\eta_1}^2 - \Delta_1}} = \sqrt{\tfrac{1}{2}[B+R] \mp \sqrt{\tfrac{1}{4}[B-R]^2 + (N-2)R_1 R_3^2}}.$$

Regrouping the expressions for η_1 and $\eta_1^2 - \Delta_1$ using these factors yields

$$\omega_{1^-} = \sqrt{\tfrac{1}{2}[B+R] + \tfrac{1}{2}[B-R](1+x')^{1/2}},$$
$$\omega_{1^+} = \sqrt{\tfrac{1}{2}[B+R] - \tfrac{1}{2}[B-R](1+x')^{1/2}},$$

where

$$x' = \frac{(N-2)R_1 R_3^2}{\frac{1}{4}(B-R)^2}$$

is small. Similar to the $[N]$ sector, the two frequencies $\omega_{1^\pm}$ in the $[N-1, 1]$ sector split into a frequency ω_{1^-}, which has a leading term B with a strong dependence on the interparticle interaction potential $\bar{V}_0$, and a frequency ω_{1^+}, in which B cancels out, leaving a leading term R that depends on the centrifugal terms. The powers of x' introduce higher-order terms

$$\omega_{1^-} \approx \sqrt{B} = \sqrt{a-b} = \sqrt{G_a F_a - G_a F_b}, \tag{D4}$$

$$\omega_{1^+} \approx \sqrt{R} = \sqrt{g + (N-4)h - (N-3)\iota} = \sqrt{G_g + (N-4)G_h} \times \sqrt{F_g + (N-4)F_h - (N-3)F_\iota}. \tag{D5}$$

APPENDIX E: ANALYSIS OF THE $[N-2, 2]$ SECTOR FREQUENCY

The frequency $\bar{\omega}_2$ associated with the root λ_2 of multiplicity $N(N-3)/2$ is given by

$$\bar{\omega}_2 = \sqrt{g - 2h + \iota}. \tag{E1}$$

Substituting the definitions of g, h, and ι in terms of F and G elements, the terms in the expression for $\bar{\omega}_2$ can be factored as

$$\bar{\omega}_2 = \sqrt{[G_g - 2G_h][F_g - 2F_h + F_\iota]}. \tag{E2}$$

Note that the only term F_g that has an explicit dependence on $\bar{V}_0$ has only a weak dependence, while F_h and F_ι contain contributions from the centrifugal potential. As $\bar{V}_0$ approaches unitarity, this frequency decreases, becoming a tiny fraction of the trap frequency.

APPENDIX F: LIMITS FOR THE FREQUENCIES AT THE INDEPENDENT-PARTICLE LIMIT

The formulas for the five frequencies from Sec. IV are summarized by

$$\bar{\omega}_{0^\pm} = \sqrt{\eta_0 \mp \sqrt{{\eta_0}^2 - \Delta_0}},$$
$$\bar{\omega}_{1^\pm} = \sqrt{\eta_1 \mp \sqrt{{\eta_1}^2 - \Delta_1}},$$
$$\bar{\omega}_2 = \sqrt{g - 2h + \iota}, \tag{F1}$$

where the variables η_0, Δ_0, η_1, and Δ_1 are defined in Eqs. (C2) and (D2), in terms of the quantities a, b, c, d, e, f, g, h, and ι given in Appendix B in terms of the F and G elements of the first-order Hamiltonian.

At the independent-particle limit, also referred to as the noninteracting limit, $\bar{V}_0 = 0$, $\gamma_\infty = 0$, and $\bar{r}_\infty = 1/\sqrt{2}$. Substituting these values into the F and G elements readily gives

$$F_a = 4, \quad G_a = 1,$$
$$F_b = 0, \quad G_g = 4,$$
$$F_e = 0, \quad G_h = 0,$$
$$F_f = 0,$$
$$F_g = 1,$$
$$F_h = 0,$$
$$F_\iota = 0.$$

Substituting these values into the expressions for a, b, c, d, e, f, g, h, and ι yields

$$\begin{aligned}
a &= G_a F_a = 4,\\
b &= G_a F_b = 0,\\
c &= G_g F_e + (N-2) G_h (F_e + F_f) = 0,\\
d &= G_g F_f + 2 G_h [F_e + (N-3) F_f] = 0,\\
e &= G_a F_e = 0,\\
f &= G_a F_f = 0,\\
g &= G_g F_g + 2(N-2) G_h F_h = 4,\\
h &= G_g F_h + G_h F_g + (N-2) G_h F_h + (N-3) G_h F_\iota = 0,\\
\iota &= G_g F_\iota + 4 G_h F_h + 2(N-4) G_h F_\iota = 0,
\end{aligned}$$

which gives, for η_0, Δ_0, η_1, and Δ_1,

$$\begin{aligned}
\eta_0 &= 4,\\
\Delta_0 &= 16,\\
\eta_1 &= 4,\\
\Delta_1 &= 16,
\end{aligned}$$

yielding a value of 2 for each frequency [see Eqs. (F1)] in units of the trap frequency as expected.

APPENDIX G: LIMITS FOR THE ANALYTIC ANGULAR FREQUENCIES FOR LARGE VALUES OF $\bar{V}_0$

Now consider the strength of the interparticle interaction $\bar{V}_0$ increasing from the weak interactions of the BCS regime to the strong interactions of unitarity. In the expanded view in the region of weak interactions in Figs. 3(a)–3(c), one can see these angular frequencies ω_{0^+}, ω_{1^+}, and ω_2 separate as the interaction gets stronger and in Figs. 5(a) and 5(b) stabilize at multiples of the trap frequency. What is happening in the analytic expressions as $\bar{V}_0$ is increasing for fixed N to yield these stable limits?

In this Appendix, I will use the analytic expressions for these three frequencies to derive these limits, working with the roots $\lambda_\alpha = \omega_\alpha^2$ in order to avoid the square-root signs in the formulas. The three angular roots λ_{0^+}, λ_{1^+}, and λ_2 are given in terms of the F and G elements by

$$\begin{aligned}
\lambda_{0^+} &= [G_g + 2(N-2)G_h]\\
&\quad \times \left[F_g + 2(N-2)F_h + \frac{(N-2)(N-3)}{2} F_\iota\right], \qquad \text{(G1)}\\
\lambda_{1^+} &= [G_g + (N-4)G_h]\\
&\quad \times [F_g + (N-4)F_h - (N-3)F_\iota], \qquad \text{(G2)}\\
\lambda_2 &= [G_g - 2G_h][F_g - 2F_h + F_\iota]. \qquad \text{(G3)}
\end{aligned}$$

Using the definitions of G_g, G_h, F_g, F_h, and F_i found in Appendix B and letting $\bar{V}_0$ become large, a little numerical work reveals that the dominant terms will involve powers of $N\gamma_\infty$, which limits to a value of -1 as $\bar{V}_0 \to 1.0$. Since $\gamma_\infty \to O(-1/N)$ for ensemble sizes relevant to experiment, extra factors of γ_∞ in a term will make it drop out. These limits for $N\gamma_\infty$ and γ_∞ are easily determined numerically and shown in Figs. 6(a) and 6(b) for two values of N. Similarly, limits for $\tanh\Theta_\infty$ and $\mathrm{sech}^2\Theta_\infty$ as $\bar{V}_0$ increases to unitarity can also be obtained numerically,

$$\begin{aligned}
\gamma_\infty &\to O\left(-\frac{1}{N}\right),\\
N\gamma_\infty &\to -1,\\
\mathrm{sech}^2\Theta_\infty &\to 0,\\
\tanh\Theta_\infty &\to 1,
\end{aligned}$$

as $\bar{V}_0 \to 1.0$.

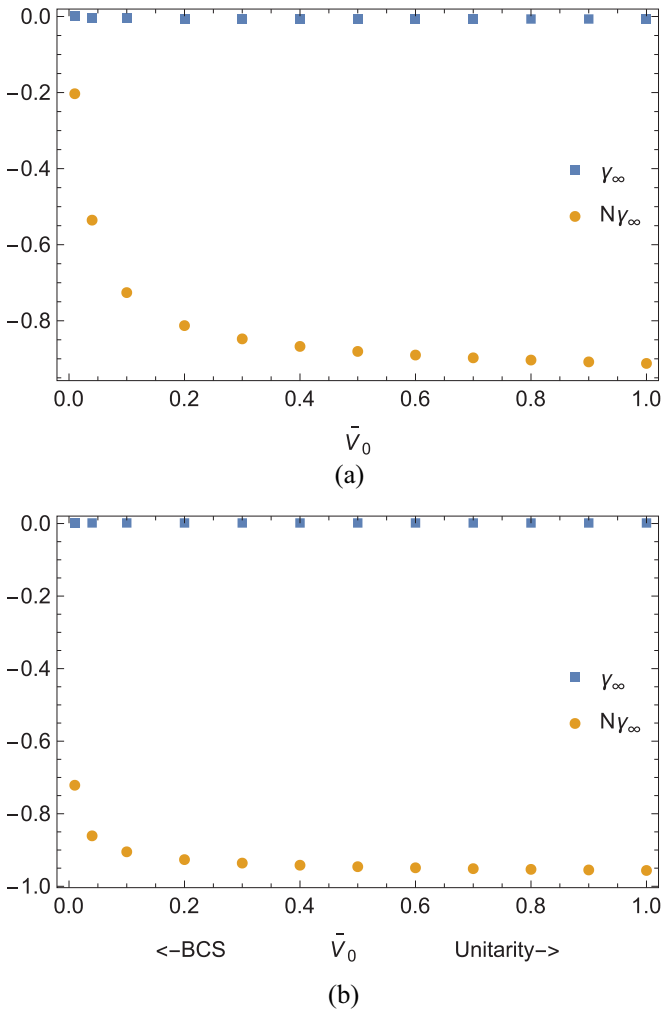

FIG. 6. Limits of γ_∞ and $N\gamma_\infty$ as a function of $\bar{V}_0$ for (a) $N = 100$ and (b) $N = 1000$.

Note that the powers of $N\gamma_\infty$ in the analytic expressions for the angular frequencies can begin to dominate the expressions in two ways. (1) As $\bar{V}_0$ increases, the magnitude of γ_∞ increases, driving $N\gamma_\infty$ towards its limit of -1 as N remains fixed. (2) Letting N increase for a fixed value of $\bar{V}_0$ will also drive $N\gamma_\infty$ towards its limit of -1. This explains the earlier observation that increasing the interaction between a fixed number of particles or increasing the number of particles experiencing a fixed interaction has a similar effect in separating the frequencies quickly. The microscopic dynamics are however distinct between the two, as discussed in Sec. VI D.

Using the above limits and the relation $\bar{r}_\infty = \frac{1}{\sqrt{2}\sqrt{1+(N-1)\gamma_\infty}}$, in the definitions of G_g, G_h, F_g, F_h, and F_i in Appendix B and keeping powers of γ_∞ that will contribute when factors of $(N-2)$, $(N-4)$, etc., are included from the expressions for the roots λ_{0^+}, λ_{1^+}, and λ_2, the limits for these G and F elements for values of N typical of experiments are

$$\begin{aligned}
G_a &= \mathbf{1},\\
G_g &= 2\frac{1-\gamma_\infty^2}{\bar{r}_\infty^2} \to \frac{\mathbf{2}}{\bar{\boldsymbol{r}}_\infty^{\mathbf{2}}},\\
G_h &= \frac{\gamma_\infty(1-\gamma_\infty)}{\bar{r}_\infty^2} \approx \frac{\gamma_\infty}{\bar{\boldsymbol{r}}_\infty^{\mathbf{2}}},
\end{aligned} \tag{G4}$$

$$\begin{aligned}
F_g &= \frac{1}{2\bar{r}_\infty^2(1-\gamma_\infty)^3[1+(N-1)\gamma_\infty]^3}\\
&\quad\times[1+3(N-2)\gamma_\infty+(13-11N+3N^2)\gamma_\infty^2\\
&\quad+(N-2)(4-3N+N^2)\gamma_\infty^3]+\frac{\bar{V}_0\bar{c}_0}{2}\operatorname{sech}^2\Theta_\infty\\
&\quad\times\left[\frac{\bar{c}_0\bar{r}_\infty^2}{1-\gamma_\infty}\tanh\Theta_\infty+\frac{\bar{r}_\infty}{2(1-\gamma_\infty)^{3/2}}\right]\\
&\to \frac{1}{2\bar{r}_\infty^2(1-\gamma_\infty)^3[1+(N-1)\gamma_\infty]^3}\\
&\quad\times(1+3N\gamma_\infty+3N^2\gamma_\infty^2+N^3\gamma_\infty^3)\\
&= \frac{1}{2\bar{r}_\infty^2(1-\gamma_\infty)^3[1+(N-1)\gamma_\infty]^3}(1+N\gamma_\infty)^3\\
&\approx \frac{\mathbf{1}}{\mathbf{2}\bar{\boldsymbol{r}}_\infty^{\mathbf{2}}},
\end{aligned} \tag{G5}$$

$$\begin{aligned}
F_h &= \frac{-\gamma_\infty}{4\bar{r}_\infty^2(1-\gamma_\infty)^3[1+(N-1)\gamma_\infty]^3}\\
&\quad\times[3+(5N-14)\gamma_\infty+(11-9N+2N^2)\gamma_\infty^2]\\
&\to \frac{-\gamma_\infty}{4\bar{r}_\infty^2(1-\gamma_\infty)^3[1+(N-1)\gamma_\infty]^3}\\
&\quad\times[3+5N\gamma_\infty+2N^2\gamma_\infty^2]\\
&= \frac{-\gamma_\infty}{4\bar{r}_\infty^2(1-\gamma_\infty)^3[1+(N-1)\gamma_\infty]^3}\\
&\quad\times[(3+2N\gamma_\infty)(1+N\gamma_\infty)]\\
&\approx \frac{-\gamma_\infty}{4\bar{r}_\infty^2(1-\gamma_\infty)^3[1+(N-1)\gamma_\infty]^2}\\
&\approx -\boldsymbol{\gamma}_\infty\bar{\boldsymbol{r}}_\infty^{\mathbf{2}},
\end{aligned} \tag{G6}$$

$$\begin{aligned}
F_i &= \frac{\gamma_\infty^2[2+(N-2)\gamma_\infty]}{\bar{r}_\infty^2(1-\gamma_\infty)^3[1+(N-1)\gamma_\infty]^3}\\
&\to \frac{\gamma_\infty^2 8\bar{r}_\infty^6}{\bar{r}_\infty^2(1-\gamma_\infty)^3} = \frac{8\gamma_\infty^2\bar{r}_\infty^4}{(1-\gamma_\infty)^3}\\
&\approx \mathbf{8}\boldsymbol{\gamma}_\infty^{\mathbf{2}}\bar{\boldsymbol{r}}_\infty^{\mathbf{4}}.
\end{aligned} \tag{G7}$$

Looking at the expressions for the three angular roots λ_{0^+}, λ_{1^+}, and λ_2, the following combinations are needed: $G_g+2(N-2)G_h$, $G_g+(N-4)G_h$, G_g-2G_h, $2(N-2)F_h$, $\frac{(N-2)(N-3)}{2}F_i$, $(N-4)F_h$, and $(N-3)F_i$. Taking these limits gives

$$\begin{aligned}
G_g+2(N-2)G_h &= 2\frac{1-\gamma_\infty^2}{\bar{r}_\infty^2}+2(N-2)\frac{\gamma_\infty(1-\gamma_\infty)}{\bar{r}_\infty^2}\\
&= \frac{2}{\bar{r}_\infty^2}(1-\gamma_\infty)[1+(N-1)\gamma_\infty]\\
&= \frac{1-\gamma_\infty}{\bar{r}_\infty^4} \approx \frac{\mathbf{1}}{\bar{\boldsymbol{r}}_\infty^{\mathbf{4}}},\\
G_g+(N-4)G_h &= 2\frac{1-\gamma_\infty^2}{\bar{r}_\infty^2}+(N-4)\frac{\gamma_\infty(1-\gamma_\infty)}{\bar{r}_\infty^2}\\
&= \frac{1-\gamma_\infty}{\bar{r}_\infty^2}[2+(N-2)\gamma_\infty]\\
&\approx \frac{\mathbf{1}}{\bar{\boldsymbol{r}}_\infty^{\mathbf{2}}},\\
G_g-2G_h &= 2\frac{1-\gamma_\infty^2}{\bar{r}_\infty^2}-2\frac{\gamma_\infty(1-\gamma_\infty)}{\bar{r}_\infty^2}\\
&= \frac{2}{\bar{r}_\infty^2}[(1-\gamma_\infty^2)-\gamma_\infty(1-\gamma_\infty)]\\
&= \frac{2(1-\gamma_\infty)}{\bar{r}_\infty^2} \approx \frac{\mathbf{2}}{\bar{\boldsymbol{r}}_\infty^{\mathbf{2}}},\\
2(N-2)F_h &\approx 2(N-2)(-\gamma_\infty\bar{r}_\infty^2) \approx \mathbf{2}\bar{\boldsymbol{r}}_\infty^{\mathbf{2}},\\
\frac{(N-2)(N-3)}{2}F_i &= \frac{N^2-5N+6}{2}F_i \approx \mathbf{4}\bar{\boldsymbol{r}}_\infty^{\mathbf{4}},\\
(N-4)F_h &= (N-4)(-\gamma_\infty\bar{r}_\infty^2) = \bar{\boldsymbol{r}}_\infty^{\mathbf{2}},\\
(N-3)F_i &\approx (N-3)8\gamma_\infty^2\bar{r}_\infty^4\\
&\approx -\mathbf{8}\boldsymbol{\gamma}_\infty\bar{\boldsymbol{r}}_\infty^{\mathbf{4}}.
\end{aligned} \tag{G8}$$

Substituting these results into the expressions for the roots (G1)–(G3) gives

$$\begin{aligned}
\lambda_{0^+} &= \frac{1}{\bar{r}_\infty^4}\left[\frac{1}{2\bar{r}_\infty^2}+2\bar{r}_\infty^2+4\bar{r}_\infty^4\right]\\
&\approx 4,
\end{aligned} \tag{G9}$$

$$\begin{aligned}
\lambda_{1^+} &= \frac{1}{\bar{r}_\infty^2}\left[\frac{1}{2\bar{r}_\infty^2}+\bar{r}_\infty^2+8\gamma_\infty\bar{r}_\infty^4\right]\\
&= \frac{1}{2\bar{r}_\infty^4}+1+8\gamma_\infty\bar{r}_\infty^2\\
&\approx 1,
\end{aligned} \tag{G10}$$

$$\begin{aligned}
\lambda_2 &= \frac{2}{\bar{r}_\infty^2}\left[\frac{1}{2\bar{r}_\infty^2}+2\gamma_\infty\bar{r}_\infty^2+8\gamma_\infty^2\bar{r}_\infty^4\right]\\
&= \frac{1}{\bar{r}_\infty^4}+4\gamma_\infty+16\gamma_\infty^2\bar{r}_\infty^2 \approx \frac{1}{\bar{r}_\infty^4}\\
&\approx O(10^{-4}) \quad \text{for the unitary regime,}
\end{aligned} \tag{G11}$$

yielding values for ω_{0^+}, ω_{1^+}, and ω_2 of

$$\omega_{0^+} = 2,$$
$$\omega_{1^+} = 1, \quad \omega_2 = O(10^{-2}) \tag{G12}$$

in units of the trap frequency $\omega_{\rm ho}$. Thus, as expected from physical arguments (see Sec. VI), these expressions for the angular frequencies limit to multiples of the trap frequency as $\bar{V}_0$ and/or N increase.

[1] M. Greiner, C. A. Regal, and D. S. Jin, Nature (London) **426**, 537 (2003).
[2] M. W. Zwierlein, C. A. Stan, C. H. Schunck, S. M. F. Raupach, S. Gupta, Z. Hadzibabic, and W. Ketterle, Phys. Rev. Lett. **91**, 250401 (2003).
[3] S. Jochim, M. Bartenstein, A. Altmeyer, G. Hendl, S. Riedl, C. Chin, J. H. Denschlag, and R. Grimm, Science **302**, 2101 (2003).
[4] J. Kinast, S. L. Hemmer, M. E. Gehm, A. Turlapov, and J. E. Thomas, Phys. Rev. Lett. **92**, 150402 (2004).
[5] T. Bourdel, L. Khaykovich, J. Cubizolles, J. Zhang, F. Chevy, M. Teichmann, L. Tarruell, S. J. J. M. F. Kokkelmans, and C. Salomon, Phys. Rev. Lett. **93**, 050401 (2004).
[6] C. A. Regal, M. Greiner, and D. S. Jin, Phys. Rev. Lett. **92**, 040403 (2004).
[7] M. W. Zwierlein, C. A. Stan, C. H. Schunck, S. M. F. Raupach, A. J. Kerman, and W. Ketterle, Phys. Rev. Lett. **92**, 120403 (2004).
[8] C. Chin, M. Bartenstein, A. Altmeyer, S. Riedl, S. Jochim, Hecker-Denschlag, and R. Grimm, Science **305**, 1128 (2004).
[9] G. B. Partridge, K. E. Strecker, R. I. Kamar, M. W. Jack, and R. G. Hulet, Phys. Rev. Lett. **95**, 020404 (2005).
[10] J. Bardeen, L. N. Cooper, and J. R. Schrieffer, Phys. Rev. **108**, 1175 (1957).
[11] A. J. Leggett, in *Modern Trends in the Theory of Condensed Matter*, edited by A. Pękalski and J. A. Przystawa, Proceedings of the XVIth Karpacz Winter School of Theoretical Physics, Karpacz, 1979 (Springer, Berlin, 1980), pp. 13–27.
[12] A. J. Leggett, Rev. Mod. Phys. **73**, 307 (2001).
[13] D. M. Eagles, Phys. Rev. **186**, 456 (1969).
[14] P. Nozieres and S. Schmitt-Rink, J. Low Temp. Phys. **59**, 195 (1985).
[15] S. Giorgini, L. P. Pitaevskii, and S. Stringari, Rev. Mod. Phys. **80**, 1215 (2008).
[16] M. Randeria and E. Taylor, Annu. Rev. Condens. Matter Phys. **5**, 209 (2014).
[17] D. L. Rousseau, R. T. Bauman, and S. P. S. Porto, J. Raman Spectrosc. **10**, 253 (1981).
[18] M. J. Clement, Astrophys. J. **249**, 746 (1981).
[19] N. Žagar, J. Boyd, A. Kasahara, J. Tribbia, E. Källén, H. Tanaka, and J.-I. Yano, Bull. Amer. Meteor. Soc. **97**, ES125 (2016).
[20] S. C. Webb, Geophys. J. Int. **174**, 542 (2008).
[21] B. V. Sanchez, J. Mar. Geodesy **31**, 181 (2008).
[22] J. Lee, K. T. Crampton, N. Tallarida, and V. A. Apkarian, Nature (London) **568**, 78 (2019).
[23] L. Fortunato, EPJ Web Conf. **178**, 02017 (2018).
[24] E. C. Dykeman and O. F. Sankey, J. Phys.: Condens. Matter **22**, 423202 (2010).
[25] M. Coughlin and J. Harms, Phys. Rev. D **90**, 042005 (2014).
[26] K. D. Kokkolas, Class. Quantum Grav. **8**, 2217 (1991).
[27] R. M. Stratt, Acc. Chem. Res. **28**, 201 (1995).
[28] C. R. McDonald, G. Orlando, J. W. Abraham, D. Hochstuhl, M. Bonitz, and T. Brabec, Phys. Rev. Lett. **111**, 256801 (2013); F. Dalfove, S. Giorgini, L. P. Pitaevskii, and S. Stringari, Rev. Mod. Phys. **71**, 463 (1999); D. Jaksch, C. Bruder, J. I. Cirac, C. W. Gardiner, and P. Zoller, Phys. Rev. Lett. **81**, 3108 (1998); H. Dong, W. Zhang, L. Zhou, and Y. Ma, Sci. Rep. **5**, 15848 (2015).
[29] H. C. Nagerl, C. Roos, H. Rohde, D. Leibfried, J. Eschner, F. Schmidt-Kaler, and R. Blatt, Fortschr. Phys. **48**, 623 (2000).
[30] D. K. Watson, Ann. Phys. (NY) **419**, 168219 (2020).
[31] B. A. McKinney, M. Dunn, D. K. Watson, and J. G. Loeser, Ann. Phys. (NY) **310**, 56 (2003).
[32] M. Dunn, D. K. Watson, and J. G. Loeser, Ann. Phys. (NY) **321**, 1939 (2006).
[33] B. A. McKinney, M. Dunn, and D. K. Watson, Phys. Rev. A **69**, 053611 (2004).
[34] W. B. Laing, M. Dunn, and D. K. Watson, Phys. Rev. A **74**, 063605 (2006).
[35] W. B. Laing, M. Dunn, and D. K. Watson, J. Math. Phys. **50**, 062105 (2009).
[36] W. B. Laing, D. W. Kelle, M. Dunn, and D. K. Watson, J. Phys. A: Math. Theor. **42**, 205307 (2009).
[37] M. Dunn, W. B. Laing, D. Toth, and D. K. Watson, Phys. Rev. A **80**, 062108 (2009).
[38] D. K. Watson, Phys. Rev. A **92**, 013628 (2015).
[39] D. K. Watson, Phys. Rev. A **93**, 023622 (2016).
[40] D. K. Watson, Phys. Rev. A **96**, 033601 (2017).
[41] D. K. Watson, J. Phys. B **52**, 205301 (2019).
[42] M. Dunn, T. C. Germann, D. Z. Goodson, C. A. Traynor, J. D. Morgan III, D. K. Watson, and D. R. Herschbach, J. Chem. Phys. **101**, 5987 (1994).
[43] D. K. Watson and M. Dunn, Phys. Rev. Lett. **105**, 020402 (2010).
[44] D. K. Watson and M. Dunn, J. Phys. B **45**, 095002 (2012).
[45] *Dimensional Scaling in Chemical Physics*, edited by D. R. Herschbach, J. S. Avery, and O. Goscinski (Kluwer, Dordrecht, 1992).
[46] *New Methods in Quantum Theory*, edited by C. A. Tsipis, V. S. Popov, D. R. Herschbach, and J. Avery, NATO Science Partnership Subseries: 3 (Springer Netherlands, Dordrecht, 1996), Vol. 8.
[47] D. Z. Goodson and D. K. Watson, Phys. Rev. A **48**, 2668 (1993).
[48] T. C. Germann, D. R. Herschbach, M. Dunn, and D. K. Watson, Phys. Rev. Lett. **74**, 658 (1995).
[49] D. K. Watson and D. Z. Goodson, Phys. Rev. A **51**, R5 (1995).
[50] M. Dunn and D. K. Watson, Ann. Phys. (NY) **251**, 266 (1996).
[51] M. Dunn and D. K. Watson, Ann. Phys. (NY) **251**, 319 (1996).
[52] M. Dunn and D. K. Watson, Few-Body Syst. **21**, 187 (1996).
[53] M. Dunn and D. K. Watson, in *Dimensional Scaling in Chemical Physics*, edited by D. R. Herschbach, O. Goscinski, and J. Avery (Springer, Netherlands, Dordrecht, 1993), p. 375.

[54] J. C. Carzoli, M. Dunn, and D. K. Watson, Phys. Rev. A **59**, 182 (1999).
[55] J. G. Loeser, J. Chem. Phys. **86**, 5635 (1987).
[56] S. Kais and D. R. Herschbach, J. Chem. Phys. **100**, 4367 (1994).
[57] S. Kais and R. Bleil, J. Chem. Phys. **102**, 7472 (1995).
[58] W. B. Laing, M. Dunn, and D. K. Watson, EPAPS Document No. E-JMAPAQ-50-031904.
[59] J. Avery, D. Z. Goodson, and D. R. Herschbach, Theor. Chim. Acta **81**, 1 (1991).
[60] E. B. Wilson, Jr., J. C. Decius, and P. C. Cross, *Molecular Vibrations: The Theory of Infrared and Raman Vibrational Spectra* (McGraw-Hill, New York, 1955).
[61] M. Hamermesh, *Group Theory and its Application to Physical Problems* (Addison-Wesley, Reading, 1962).
[62] L. D. Landau, Sov. Phys. JETP **3**, 920 (1957); **5**, 101 (1957).
[63] M. Bartenstein, A. Altmeyer, S. Riedl, S. Jochim, C. Chin, J. H. Denschlag, and R. Grimm, Phys. Rev. Lett. **92**, 203201 (2004).
[64] M. A. Baranov and D. S. Petrov, Phys. Rev. A **62**, 041601(R) (2000).
[65] Z. Zhen and J. Loeser, in *Dimensional Scaling in Chemical Physics*, edited by D. R. Herschbach, J. Avery, and O. Goscinski (Kluwer, Dordrecht, 1992), Chap. 3, p. 90.
[66] J. Goldstone, Nuovo Cimento **19**, 154 (1961).
[67] S. Hoinka, P. Dyke, M. G. Lingham, J. J. Kinnunen, G. M. Bruun, and C. J. Vale, Nat. Phys. **13**, 943 (2017).
[68] Y. Ohashi and A. Griffin, Phys. Rev. A **67**, 063612 (2003).
[69] P. W. Anderson, Phys. Rev. **110**, 827 (1958).
[70] P. W. Anderson, Phys. Rev. **112**, 1900 (1958).
[71] N. N. Bogoliubov, V. V. Tolmachov, and D. V. Širkov, Fortschr. Phys. **6**, 605 (1958).